

INFORMATION TO USERS

This manuscript has been reproduced from the microfilm master. UMI films the text directly from the original or copy submitted. Thus, some thesis and dissertation copies are in typewriter face, while others may be from any type of computer printer.

The quality of this reproduction is dependent upon the quality of the copy submitted. Broken or indistinct print, colored or poor quality illustrations and photographs, print bleedthrough, substandard margins, and improper alignment can adversely affect reproduction.

In the unlikely event that the author did not send UMI a complete manuscript and there are missing pages, these will be noted. Also, if unauthorized copyright material had to be removed, a note will indicate the deletion.

Oversize materials (e.g., maps, drawings, charts) are reproduced by sectioning the original, beginning at the upper left-hand corner and continuing from left to right in equal sections with small overlaps.

Photographs included in the original manuscript have been reproduced xerographically in this copy. Higher quality 6" x 9" black and white photographic prints are available for any photographs or illustrations appearing in this copy for an additional charge. Contact UMI directly to order.

ProQuest Information and Learning
300 North Zeeb Road, Ann Arbor, MI 48106-1346 USA
800-521-0600

UMI[®]

University of Alberta

Localization of the sources of the electroencephalogram

by

Angela Antoniu



A thesis submitted to the Faculty of Graduate Studies and Research in partial fulfillment of
the
requirements for the degree of *Master of Science*

Department of *Electrical and Computing Engineering*

Edmonton, Alberta

Fall 2000



National Library
of Canada

Acquisitions and
Bibliographic Services

395 Wellington Street
Ottawa ON K1A 0N4
Canada

Bibliothèque nationale
du Canada

Acquisitions et
services bibliographiques

395, rue Wellington
Ottawa ON K1A 0N4
Canada

Your file Votre référence

Our file Notre référence

The author has granted a non-exclusive licence allowing the National Library of Canada to reproduce, loan, distribute or sell copies of this thesis in microform, paper or electronic formats.

The author retains ownership of the copyright in this thesis. Neither the thesis nor substantial extracts from it may be printed or otherwise reproduced without the author's permission.

L'auteur a accordé une licence non exclusive permettant à la Bibliothèque nationale du Canada de reproduire, prêter, distribuer ou vendre des copies de cette thèse sous la forme de microfiche/film, de reproduction sur papier ou sur format électronique.

L'auteur conserve la propriété du droit d'auteur qui protège cette thèse. Ni la thèse ni des extraits substantiels de celle-ci ne doivent être imprimés ou autrement reproduits sans son autorisation.

0-612-59772-5

Canada

University of Alberta

Library Release Form

Name of Author: *Angela Antoniu*

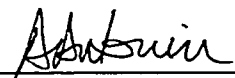
Title of Thesis: *Localization of the sources of the electroencephalogram*

Degree: *Master of Science*

Year this Degree Granted: *2000*

Permission is hereby granted to the University of Alberta Library to reproduce single copies of this thesis and to lend or sell such copies for private, scholarly, or scientific research purposes only.

The author reserves all other publication and other rights in association with the copyright in this thesis, and except as hereinbefore provided, neither the thesis nor any substantial portion thereof may be printed or otherwise reproduced in any material from whatever without the author's prior written permission.



537 RH Michener Park,

Edmonton, Alberta,

Canada, T6H 4M5

September 29, 2000

ABSTRACT

Three algorithms for localization of electrical neural activity of the brain, based on the spatio-temporal decomposition of the EEG, are explored. The EEG is decomposed in spatial and temporal components using the PC (principal component) and the CSP (common spatial pattern) decompositions. The components thought of as representing the neural activity of interest are isolated and used with the Single Dipole Fitting, MUSIC (multiple signal classification) and LORETA (low resolution electromagnetic tomography) source localization algorithms in an analytical three-shell spherical model of the head.

In a noiseless simulation example, the CSP decomposition shows to be superior to PC in isolating the sources of interest when background sources are also present, and used with MUSIC and LORETA precisely localize the sources. Applied to a seizure EEG, the seizure onset zone of the brain is estimated. The result is corroborated with the clinical findings and shows correct lateralization of the onset.

“Nil sine magno vita labore

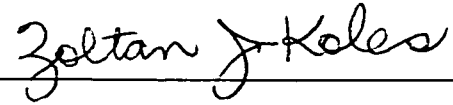
dedit mortalibus”

Horatius, “*Satirae*”

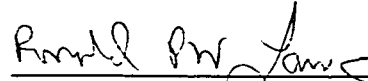
University of Alberta

Faculty of Graduate Studies and Research

The undersigned certify that they have read, and recommend to the Faculty of Graduate Studies and Research for acceptance, a thesis entitled *Localization of the sources of the electroencephalogram* submitted by *Angela Antoniu* in partial fulfillment of the requirements for the degree of *Master of Science*.



Dr. Z. J. Koles

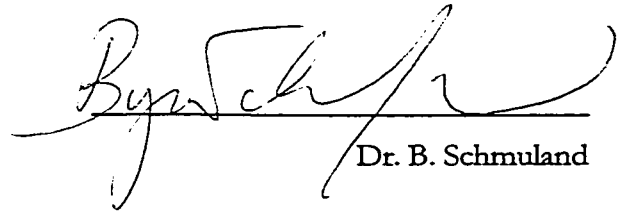


Dr. R. P. W. Lawson

Chair
only



Dr. H. Marquez



Dr. B. Schmuland

September 28, 2000

*This thesis is dedicated to my dear son
Oliver, and to my parents and best friends
Oltea and Alexandru.*

Acknowledgments

My deepest gratitude goes to all of the professors that have given me the opportunity to learn, offered me support, and contributed to my professional growth. As well, I am deeply grateful to all of the colleague students who share my belief that interdependence is higher value than independence, and from whom I have benefited through interactive learning. I am also grateful to my students for their receptivity and for giving me a sense of accomplishment.

I am grateful to my supervisor, Dr. Z.J. Koles, for accepting me to work on a project in Biomedical Engineering, which I found most meaningful, interesting and exciting. I would also like to express my appreciation for his valuable feedback while completing my thesis, and his support in publishing it.

I express my gratitude to my family, especially to my wonderful, loving son Oliver for often giving up our “special time together” so I could work, and to my parents for their unconditional love, permanent support and encouragement. I also express my appreciation to my husband for his excellent cooperation during my early research work.

Last but not least, I am grateful to my numerous friends for their encouragement, for going out of their way to help, and for being fun. Special thanks to Ion and his family for their true friendship.

TABLE OF CONTENTS

1	Introduction	1
1.1	Electroencephalography	2
1.1.1	Characteristics of the EEG.....	2
1.1.2	EEG Instrumentation	4
1.2	Brain anatomy	6
1.3	Source and Head Models.....	7
1.3.1	The Source Model.....	7
1.3.2	The Head Model.....	8
1.3.2.1	The Analytical Head Model	8
1.3.2.2	Numerical Head Models.....	10
1.3.2.2.1	Finite Element Method (FEM).....	10
1.3.2.2.2	Boundary Element Method (BEM)	11
1.3.2.2.3	Lead Field Analysis (LFA).....	12
1.4	Source Localization.....	13
2	Methods	16
2.1	EEG Spatio-Temporal Decompositions.....	16
2.1.1	The EEG model.....	16
2.1.2	The Principal Component EEG Decomposition	18
2.1.3	The Common Spatial Pattern Decomposition	22
2.2	Source Localization Methods.....	26
2.2.1	Single Dipole Fitting.....	27
2.2.2	Multiple Dipole Fitting.....	32
2.2.3	LORETA.....	36
2.3	Seizure onset (temporal) localization	43
3	Simulation Results.....	44
3.1	EEG Spatio-Temporal Decompositions.....	44
3.1.1	The EEG Model.....	44
3.1.2	The Principal Component Decomposition of the EEG.....	47
3.1.3	The Common Spatial Pattern Decomposition	50
3.2	Source Localization - Simulation Results	52
3.2.1	Single Dipole Fitting.....	53
3.2.2	Multiple Dipole Fitting.....	55
3.2.3	LORETA.....	57

3.2.4	Seizure Spread.....	58
4	Real Data Results	60
4.1	Introduction.....	60
4.2	Clinical procedure.....	61
4.3	The seizure onset and source localization procedure.....	62
4.4	Real data analysis.....	62
4.4.1	Seizure onset localization	63
4.4.1.1	Band Pass Filtering.....	64
4.4.1.2	Spatial Filtering	65
4.4.2	Source localization	70
4.4.2.1	Single Dipole Fitting	70
4.4.2.2	Multiple Dipole Fitting.....	72
4.4.2.3	LORETA.....	74
4.4.3	Seizure Spread.....	75
4.5	Validation of Results	77
5	Discussion	78
6	Conclusions	86
	Bibliography.....	88

TABLE OF FIGURES

Figure 1.1. The 25 electrode montage used for the EEG recording.	5
Figure 1.2. The spherical model and the dipole representation.....	9
Figure 3.1. The potential images produced by three sources (a) and the corresponding source currents (b).	45
Figure 3.2. The EEG (V) simulated using the spatial and temporal components plotted in Figure 3.1.	47
Figure 3.3. The Principal Component spatio-temporal decomposition. (a) The spatial patterns. (b) The temporal patterns	48
Figure 3.4. The Common Spatial Pattern Decomposition. (a) The Common Spatial Patterns; (b) The Temporal Patterns	51
Figure 3.5. The topography of the <i>SLI</i> using Single Dipole Fitting for the three sources of the simulated EEG. (a) All three eigenvectors corresponding to nonzero eigenvalues are used. (b) Only the first two eigenvectors are used.....	54
Figure 3.6. The topography of the <i>SLI</i> using Multiple Dipole Fitting for the three sources of the simulated EEG. (a) All three eigenvectors corresponding to nonzero eigenvalues are used. (b) Only the first two eigenvectors are used.....	56
Figure 3.7. (a) The topography of the <i>SLI</i> using MUSIC with CSP. (b) The Topography of the LORETA solution using CSP.	58
Figure 3.8. The dynamics of the abnormal electrical activity in the last five seconds of the EEG	59
Figure 4.1. The epoch from the recorded EEG containing the seizure onset.....	63
Figure 4.2. The power spectrum of the band pass filter used for the raw EEG filtering.....	64
Figure 4.3. The frequency filtered EEG epoch.....	65
Figure 4.4. The EEG temporal components, Z	66
Figure 4.5. The first four spatial components of the frequency filtered EEG resulted from the CSP filtering.	67
Figure 4.6. The reconstructed EEG from the first three spatio-temporal components.....	69
Figure 4.7. The First Principal Component b and its corresponding waveform	70
Figure 4.8. The reconstructed EEG from the first Principal Component b and its corresponding waveform	71
Figure 4.9. The Source Location Index distribution on the horizontal and vertical slice containing the minimum using the Single Dipole Fitting Method	72
Figure 4.10. The Source Location Index distribution on the horizontal and vertical slice containing the minimum using the Multiple Dipole Fitting Method	73
Figure 4.11. The horizontal and vertical slice topography of the LORETA solution.....	75
Figure 4.12. The <i>SLI</i> dynamics in the first four seconds of the seizure.....	76

1 INTRODUCTION

Many research groups from all over the world have been actively involved in finding improved methods for producing images of the brain activity to generate insight in basic and clinical aspects of neural processing. Imaging techniques as functional Magnetic Resonance Imaging (fMRI), Magnetic Resonance Spectroscopy (MRS), Positron Emission Tomography (PET) and Single Photon Emission Tomography (SPECT) can produce images containing important information regarding the neural activity. Some of these techniques (PET, fMRI in the same scanner) are capable of producing images with a spatial resolution on the order of millimeters (*Hammer et al.*, 1998).

On the other hand, the ElectroEncephaloGram (EEG) directly measures the scalp electric potentials produced by neural activation and has good temporal resolution, on the order of a few milliseconds, that can not be equaled by any of the mentioned imaging techniques. The temporal resolution is important as it can provide information about changes in patterns of the neural activity. Considerable research interest has been spawned by studies of the electrical activity of the human brain. Many studies examine the relationship between the location of the neural sources and the measured potentials on the scalp (EEG). These studies aim either to get more insight about which regions of the brain are activated during certain cognitive tasks, or for clinical purposes, as to determine in which region of the brain some abnormal electrical activity would occur from one point in time.

The main objective of this work is to describe and apply methods of localization of the sources of EEG, given the measurement. The methods will be applied to EEG data acquired from epileptic patients. Besides the locations, the orientations and the moments of the neural sources that become active at one point in time can be determined within a head model.

Finding the source parameters from the available EEG is called the inverse problem. This is an ill-posed problem; not only one distribution of sources can produce the measured EEG. The non-uniqueness of the solution can be overcome by imposing physical models to the neural sources, which can be modeled as dipoles or as distributions of dipoles. The dipole model is considered as accurately modeling the coherent activity of a large number of neurons (*Scherg and von Cramon, 1985*).

1.1 Electroencephalography

The word electroencephalogram (EEG) means “electrical brain picture”, coming from the Greek *electro-* electrical, *encephalo-* brain and *gram(ma)-* picture. Electroencephalography is the technique that allows the measurement of the electrical potential difference between two points on the scalp produced by the neuronal activity in the brain. Hans Berger published the first EEG in 1929. His study was based on the measurement of the potential at only one site (*Kuzniecky, et al., 1995*)

1.1.1 Characteristics of the EEG

The EEG is a set of signals (potentials) with amplitudes that vary in time and is the result of the flow of volume currents produced by the synchronized electrical activity in the brain cortex through brain, skull and scalp. The amplitude of the EEG in a normal patient is of the order of tens of microvolts or lower. The electrical activity of the normal brain generates frequencies that are divided into five frequency bands: *delta* (0.5-4 Hz), *theta* (4-8 Hz), *alpha* (8-13 Hz), *beta* (13-22 Hz) and *gamma* (22-30 Hz). The most prominent rhythm in the EEG activity of healthy adults is the alpha rhythm. It originates in the occipital region of the head and can be seen on the EEG recording when the subject is with eye closed, with visual input causing the amplitude of the alpha wave to decrease. A similar change in the alpha rhythm amplitude can

be observed during the performance of mental tasks like arithmetic. The alpha rhythm attenuates during the task performance, the amplitude being reestablished after the answer is given (Tyner et al., 1983).

The EEG recorded from humans not only contains activity which is the result of sources in the brain, but also artifacts, with sources extraneous to the brain, such as eye blinks and muscle artifacts. The eye blink artifact appears predominantly at the inferior frontal electrodes, Fp1 and Fp2 and consists of a high amplitude oscillation of very low frequency that lasts less than one second. The muscle artifact appears on the EEG as a high frequency waveform superimposed on the brain and the other artifactual activity and comes from the facial and scalp muscles.

The normal EEGs are considered as being the recordings obtained from healthy patients, with no symptoms, complaints and history of neurological disorders or other significant disease (Tyner et al., 1983). However, in unhealthy patients changes from the known normal patterns, specific to the disease, occur in the electrical activity. Only the patterns specific to the epilepsy disorders will be mentioned here.

Three periods of time are considered in the observation and processing of an EEG recorded in an epileptic patient: *interictal*, *ictal*, *postictal*. The *inter-ictal* EEG is the EEG recorded in the interval of time between two seizures and often in this work will be referred to as “*the normal EEG*” or the *pre-ictal* EEG. What it is called *ictal EEG* in epilepsy (*the abnormal EEG*) is the recording in the period of time when the patient is having a seizure. The time at which the seizure starts is called the *onset* of the seizure and is considered as the delimitation between the *pre-ictal* and *ictal* EEG, its identification being one of the main challenges in the source

localization process. It is thought that the seizure usually starts in a so-called *focus* (also referred to in the literature as *seizure focus* or *pacemaker*), at the time that corresponds to the seizure onset. The interval of the recording that corresponds to the disappearance of the patient's signs and symptoms of the seizure and the returning to his pre-ictal condition is the *postictal* EEG.

The EEG in epilepsy is characterized by certain patterns. It has been observed that in many of the epileptic subjects, the *interictal* EEG recordings show spike discharges of approximately 50 μ V, generated by irritative zones in the cortex. In the *ictal* state the patient's behavior may be altered or/and paroxysmal neuronal activity takes place within the brain. The ictal EEG is characterized by high amplitude waveforms of frequencies up to 10-12Hz, superimposed on the background EEG. The high amplitude activity may appear in bursts or as a constant pattern and it would last for seconds or more.

1.1.2 EEG Instrumentation

The scalp electroencephalogram is obtained by measuring the amplified difference in potential between sensors (electrodes) placed on the human scalp. EEG recorded on the scalp is not the only type of brain electrical recording. However, in this thesis "EEG" refers to the surface electrical recordings, if otherwise not specified.

The electrodes are attached to the scalp with a conductive gel in order to minimize the impedance between the electrode and the scalp. Ideally the electrodes are identical, and this impedance is identical between all of the electrodes and scalp. This is however difficult to achieve in practice mainly due to the differences in the electrode composition and to electrode movement. The electrodes are placed on the scalp in standard positions for each measurement. A channel in an electrode array is the potential measured between two electrodes, usually with respect to a reference electrode. When all the potentials are measured with respect to a single

reference electrode, the montage is called unipolar. Throughout this work a 25-electrode montage: 24 measurement sites with respect to a common reference CZ' located at the middle point between the standard positions of CZ and PZ is used. The electrode positions of this electrode array are shown in Figure 1.1.

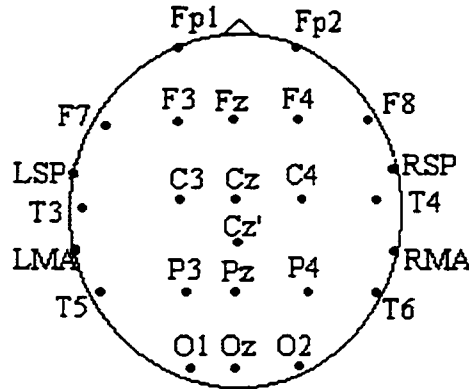


Figure 1.1. The 25 electrode montage used for the EEG recording.

The montage used is: FP1, FP2, F3, F4, C3, C4, P3, P4, O1, O2, F7, F8, T3, T4, T5, T6, FZ, CZ, PZ, LSP, RSP, LMA, RMA, OZ. LSP and RSP stand for left and right sphenoidal whereas LMA and RMA stand for left and right mastoidal; the other 20 electrodes are placed in their 10-20 international standard positions (Tyner et al., 1983). This is the electrode configuration used in the telemetric unit where the EEG data analyzed in the results chapter of this thesis was acquired.

With the development of the first digital electroencephalograph in late 80's the flexibility of the EEG systems increased. The amplified voltages acquired from the low impedance (less than $3k\Omega$) electrode array, are applied to an analog-digital converter (ADC), usually at more than 8 bit analog to digital precision to ensure high dynamic range and ADC resolution. The ADC converter is connected to a computer, offering possibilities of data storage and

manipulation. The computer interface with amplifiers, of very high input impedance, common mode rejection ratio and open loop gain, allow automatic settings and corrections of amplifier gain. The gain settings are stored and displayed along with the data, as well as the filter (0.3 to 70Hz) settings. The calibration of the channels is controlled by computer software, the gain adjustment is done such that all of the channels have the same gain. The EEG tracings therefore show the true voltages on all of the channels (*Wong, 1996*).

It is thought by Gevins that combining a few technologies, it would be possible to achieve near one millimeter precision in localizing regions of activated brain tissue and subsecond temporal precision for characterizing changes in patterns of activation over time (*Gevins, 1995, 1998*). In the attempt to achieve high spatio-temporal resolution, progress has been made in concomitantly acquiring interictal EEG and fMRI in an MRI scanner (*Ives et al., 1993, Jager et al., 1998, Krakow et al., 1998, Laxeyras et al., 1998, Symms et al., 1998*).

1.2 Brain anatomy

The main divisions of the human brain are brainstem, cerebellum and cerebrum. The structure that contributes to the generation of the EEG is the outer part of the cerebrum - the two brain hemispheres, called the cerebral cortex. The cerebral cortex, about 2-3 mm thick, with a total surface area of approximately 1600 cm² contains about 10¹⁰ neurons, or nerve cells (*Nunez et al., 1981*). It is composed of gray matter, which is an intricate fabric of interconnected neural cells (through dendrites and synapses). The layer just below the gray matter is mostly composed by nerve fibres, axons, and is called white matter. The grey matter is believed to be the main generator of the strong electrical potential measured on the scalp (*Webster, 1992 Hendelman, 1994, Myers, 1995*).

A single neuron can be covered with 10^3 - 10^5 synapses, with two types of synaptic inputs: one type produces excitatory postsynaptic potentials across the membrane of the output neuron; the other produces inhibitory postsynaptic potentials. In both cases a current flows through the local surface of the membrane, through the intracellular fluid and back to the membrane at a distance from the local surface, closing the loop at the synapse, its sense depending on the type of synaptic input. The membrane acts as a current sink or as a current source, depending on the sense of the current. The membrane surface at an instant in time is composed of sources and sinks distributed depending on the properties of the synapses, neurons and medium. On the other hand, the dendrites are distributed in a column fashion in the cerebral cortex, normal to the cortical surface. As the high number of synapses is distributed over the cell body and dendritic surface and due to the high density of neurons ($\sim 10^5/\text{mm}^2$), at any instant in time a summed current flow distribution is produced. Due to the columnar distribution of the cells this current is the result of a coherent summation of the currents of nearly synchronous activation of a small area in the cortex.

1.3 Source and Head Models

1.3.1 *The Source Model*

In the previous section the electrogenesis of the sources of EEG was explained. Considering the focal activity, the resulting current can be thought of as being produced by an equivalent dipole located approximately in the center of the small area in the cortex, with infinitely small distance between the source and the sink compared to the distance between the dipole and the measurement sites. Thus a single source can be modeled as a dipole. If the neural activity is distributed over a larger area, the neural activity can be modeled as a dipole sheet, or dipole layer, which is a set of synchronously active dipoles distributed on the area of

the brain. In this work, it is assumed that the source model does not change its location or orientation during an EEG measurement.

In order to explain the relationship between these sources and the EEG measured on the scalp, knowledge about the medium between the source and the electrode sites is necessary. An important feature of a dipole is that it produces a potential in the surrounding medium that falls off as the inverse square of the distance. This inverse square law holds only in an infinite homogeneous medium (Nunez et al., 1981).

1.3.2 The Head Model

In order to perform the localization of the neural sources it is necessary to determine the potentials produced on the scalp by unit moment current sources. This is called the *forward problem*.

In order to be able to calculate the potential produced on the scalp by a unit dipole source, a mathematical description of the volume conductor is required. This mathematical description can be either analytical, or numerical. First the analytical model is presented. A review of the numerical methods of head modeling will be made afterward.

1.3.2.1 The Analytical Head Model

The head model that was used in the present work is an analytical model, a three shell spherical model, with three regions of constant conductivity: brain, skull and scalp. The radii of the shells are in order: r_1, r_2 and R . Each shell is considered homogenous. The conductivity of the neural and scalp tissue is considered the same, σ , and the conductivity of the skull is σ_s . This model was first developed by Ary et al., 1981, for the restricted case of dipoles on the z axis, oriented in only one plane. The coordinate system for dipoles in the spherical model is

represented in Figure 1.2. For the sake of simplicity, the radii r_1, r_2 are not represented in the figure.

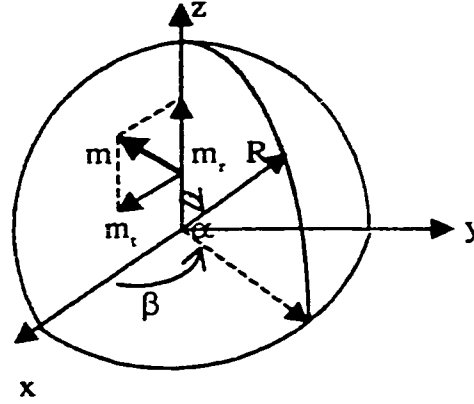


Figure 1.2. The spherical model and the dipole representation

The potential $V(\alpha, \beta)$, produced by the dipole m , placed on the z -axis and oriented in the positive xz plane, at one point on the surface of the inhomogeneous spherical head model (of radius R) can be calculated using the equation

$$V(\alpha, \beta) = \frac{1}{4\pi\sigma} \sum_{n=1}^{\infty} \frac{2n+1}{n} b^{n-1} \left[\frac{\xi(2n+1)^2}{d_n(n+1)} \right] \cdot [nm_r P_n(\cos\alpha) + m_t P_n^1(\cos\alpha) \cos\beta],$$

where $b = \frac{z}{R}$ is the eccentricity of the dipole m , m_r and m_t are the radial and tangential components of the dipole moment, $\xi = \sigma_s/\sigma$ is the ratio between the conductivity of the skull tissue, σ_s , and the soft tissue (brain and scalp), σ ; $P_n(\cos\alpha)$ and $P_n^1(\cos\alpha)$ are the Legendre polynomials.

$$d_n = [(n+1)\xi + n] \cdot \left[\frac{n\xi}{n+1} + 1 \right] + (1-\xi) \cdot [(n+1)\xi + n] \cdot (f_1^{2n+1} - f_2^{2n+1}) - n(1-\xi)^2 \left(\frac{f_1}{f_2} \right)^{2n+1}$$

where $f_1 = \frac{r_1}{R}$ and $f_2 = \frac{r_2}{R}$.

The model used in this work allows the calculation of the potential everywhere on the surface of the head created by a dipole of arbitrary orientation, placed at any location in the inner sphere. However, only the equation of the potential given by *Ary et al.* is given here, showing the potential created by the dipole on the outer sphere.

1.3.2.2 Numerical Head Models

The numerical models of the head aim to incorporate more information about the geometric and structural features of the head of the studied patient. This information increases the accuracy of the localization in comparison to the three shell spherical model used in this thesis.

A number of methods for calculating the potentials on the surface of a realistic head have been developed. The FEM (Finite Element Method) and the BEM (Boundary Element Method) are the most commonly used.

1.3.2.2.1 Finite Element Method (FEM)

Three-dimensional finite element models provide a method to study the relationship between human scalp potentials and neural current sources inside the brain (*Yan et al.*, 1991). The FEM is based on the conductivity distribution within the head, which can be collected from a stack of MRI slices, or, as suggested by *Haueisen et al.* in 1995, by superimposing MRI and CT in order to improve the tissue segmentation. The idea of implementing this method consists of modeling the head as a 3-D n-sized network of resistors, where the voltage at each

node is unknown. In the 3-D network, each node can be connected to at most six other nodes. Each node defines an equation that can have at most seven unknowns and there will be n^3 equations, one for each node. The matrix that contains all of the values of the resistors between the nodes is formed. Depending on the sense of the current in each node, the matrix will be positive definite or negative definite and symmetric. If the algebraic sum of all of the currents in a node is zero, no current source can be located at that node.

The set of equations that must be solved is:

$$\mathbf{A}\mathbf{v} = \mathbf{i}$$

where \mathbf{A} is the matrix of conductivities, \mathbf{v} is the vector of node voltages, and \mathbf{i} is the current vector containing the sources and the sinks of the dipole sources. The indices of each voltage node indicate its position in the network. If a distance is assigned to each index, the indices will indicate the distance from an established reference point. The challenge of this method is computing the inverse of the large matrix \mathbf{A} .

1.3.2.2.2 *Boundary Element Method (BEM)*

The BEM is a computational technique, which uses Green's Theorem to transform the differential equation describing the potential distribution within a volume conductor into an integral equation over the boundary surfaces between regions with different electrical properties. The construction of the real head model is based on MRI data. After the acquisition of a set of MRI slices of the head, a sequential view is taken in order to reconstruct the MRI image of the head. The three surfaces (scalp, skull and brain) of the head are then digitized, sampling the three contours of each slice (*Roth et al., 1993, Fletcher et al., 1995*). The use of the sampled surfaces as they are to perform numerical calculations would be too

computationally demanding so that sets of sampled points can be grouped, more often the three surfaces resulting in sums of triangles, although quadrilateral boundary elements could be used (*Brebbia et al*, 1980).

The BEM requires only surface meshes of the different head structures: scalp, skull and brain. The potential differences on these surfaces can be calculated using an approximation of the integral equations that characterize the potential on the surface by a system of linear equations of the form

$$\mathbf{B}\mathbf{v} = \mathbf{g}$$

where \mathbf{v} is a vector of length N containing the values of the potential at each center of mass of every element, \mathbf{g} is a vector of length N describing the dipole source terms, and \mathbf{B} is an $N \times N$ matrix, N being the number of total elements of the model, which does not depend on the dipole source, involving solid angles under which each triangle of each surface sees every other triangle. N^2 solid angles will result (*Alibadi et al*, 1993, *Fletcher et al*, 1995).

Yvert et al., in 1995, developed a method of improving the numerical accuracy by using locally refined meshes such that the solid angle of each element subtended at the source location was constant. This work considers the influence of the dipole depth and the improvement brought by local mesh refinement. The terms "global mesh density" and "local mesh density" were introduced to define the number of triangles per cm^2 .

1.3.2.2.3 *Lead Field Analysis (LFA)*

The LFA algorithm is a computational technique for the calculation of potentials on the surface of a realistically shaped volume conductor model based on the Boundary Element

Method. *Fletcher et al.* shows that this method is superior to BEM from the point of view that it yields more accurate surface potentials for a wider range of dipole locations. This method is less computationally costly and the amount of data that needs to be stored is considerably reduced.

1.4 Source Localization

Localization of the neural activity in the brain is important clinically especially for surgical candidates. In the case of epilepsy for example, the decision regarding the area of the brain that has to be removed is made based on the information regarding the location of the seizure focus. Imaging methods, mostly MRI, are currently used as clinical tools in the pre-surgical localization of epileptic activity, in the attempt to detect the regions of the brain that are structurally or functionally abnormal (*Arnold, 1993, Cascino, 1995, Kuźnietsky et al., 1995, Desjortova et al., 1998, Lin et al., 1998, Shen et al., 1998*). In some cases, with structural abnormalities, the zone of the abnormal tissue is highly suspected as being responsible for the abnormal patterns in the EEG, and are removed. However, the success consists in removing the seizure focus, and sometimes removing the abnormal tissue gives only temporary results. MRS can provide direct biochemical information from within the cell. This imaging method might be important for source localization, in spite of the poor temporal and spatial resolution, as the source current is dependent on the diffusion of a chemical (transmitter) from the synapses through the subsynaptic membrane.

The source localization based on EEG data requires both reliability and resolution. The sources are considered as produced by current dipoles in a three-shell sphere, and a unit dipole model can be calculated at any point in the head model. In order to determine the neural source parameters, the EEG is often decomposed into spatial and temporal patterns (*Scherg et*

al., 1986, *Koles*, 1991, 1997, *Mosher et al.*, 1992, *Koles et al.*, 1995, *Soong et al.*, 1995, *van Drongelen et al.*, 1997, *Koles et al.*, 1998, *Mosher et al.*, 1998). The problem is that the number of sources of EEG can be greater than the number of measurement sites.

The EEG contains both spatial and temporal patterns that are of interest and spatial and temporal patterns that are not of interest for source localization and can be modeled as noise. The separation of the spatial and temporal patterns of interest is a challenge especially in the presence of noise. However, if this separation is done and the EEG is reconstructed from estimated spatial and temporal patterns corresponding to the neural activity of interest, the source parameters for these sources can be found by finding the best fit (minimum error) between the EEG model and this EEG. An alternative method to localizing the sources based on the dipole fitting is calculating the smoothest solution for the current density distribution in the head volume.

In this work, a method that calculates the current density distribution in the head volume, called LORETA, is applied to multiple time slices. Also, two methods of separating the signal components from the noise spatial and temporal components, based on the analysis of the covariance matrix of the EEG, are demonstrated, applied and compared. The decompositions are incorporated in source localization algorithms, which are compared for effectiveness.

This thesis aims to conclude about which developed methods of source localization, modified to incorporate two types of EEG decomposition, give accurate localization of simulated sources and if the methods give relevant results in analyzing real data using a spherical model of the head. In the future, more realistic head models, that better describe the volume conductor, based on information from MRI and CT, can be developed and used in the

localization methods, in the attempt to obtain increased accuracy in estimating the locations of the neural sources of interest.

2 METHODS

The source localization problem involves the estimation of the source parameters (locations, orientations, and magnitudes) that produced the measured scalp electric potentials. In order to estimate these parameters the measured scalp potentials are modeled. Chapter 2.1 describes the method of modeling the EEG. Using this model, the source parameters are determined. Three source localization methods are presented in Chapter 2.2.

2.1 EEG Spatio-Temporal Decompositions

The EEG is a complex signal, with statistical properties depending on space and time. It is usually assumed that the EEG samples are normally distributed, and, for this reason, the statistics of the normal distributions can be used in EEG analysis.

2.1.1 *The EEG model*

Let the potential measured at N electrode sites be $\mathbf{V}(t)=[V(t_1), V(t_2), \dots, V(t_t), \dots, V(t_T)]$, where $\mathbf{V}(t)$ is the N dimensional instantaneous potential vector recording at time sample t . The recording progresses for $t = \overline{1, T}$ samples. Consequently, \mathbf{V} will be a matrix of dimension $N \times T$.

As mentioned before, the recorded potential \mathbf{V} can be decomposed into spatial and temporal components using physical models that incorporate the head models and neural source models, with the neural source model a current dipole. The current dipole is assumed to be in a fixed position and orientation and has variable magnitude during the recording. The head model is assumed to be a purely conductive medium and the transfer coefficient between a dipole at some location, with some orientation, and an electrode placed at a specific location on the head model surface represents the potential produced at the electrode by a unit strength dipole. This is known as the forward problem in EEG. The transfer coefficient is calculated using the head model, in the present work a three-shell spherical model, with three regions of

conductivity: In this case the potential produced by a dipole can be computed analytically as in section 1.3.2.1.

With these assumptions, the potential variation in time, at any electrode site $n = \overline{1, N}$, with $T > N$, can be modeled as a linear combination of the transfer coefficients m , between the $l = \overline{1, L}$ active source generators and the electrode n , and the variation of the dipole source magnitude in time:

$$v_n(t) = \sum_{l=1}^L m_{nl} s_l(t) + e_n(t) \quad 2.1$$

$e_n(t)$ is the additive, zero mean Gaussian random noise term that may be measured at the electrode site n . Since the head is assumed to be purely conductive, any current dipole source l will produce potentials at the N electrodes on the scalp which will be in phase with the source current $s_l(t)$. The formula is the spatio-temporal decomposition of the potential at electrode n . In matrix form, the measured $V(t)$ can be expressed as

$$\mathbf{V} = \mathbf{MS} + \mathbf{E} \quad 2.2$$

\mathbf{M} represents the $N \times L$ source image matrix on the scalp for the L unit dipole sources. \mathbf{S} is the $L \times T$ source current matrix and \mathbf{E} is the N by T noise matrix and is also the error between the measured \mathbf{V} and the potentials produced by the L dipole sources. Each column of \mathbf{M} in this formula is the vector sum of three calculated unit source vector components, \mathbf{M}_x , \mathbf{M}_y , \mathbf{M}_z , that share the same location in the Cartesian coordinate system X, Y, Z . In the spherical head model, the origin of the coordinate system is placed in the center of the spheres; X is oriented towards the right ear, Y towards naision and Z towards the top of the head.

The matrix form of the spatio-temporal model presented incorporates the spatial (**M**) and the intensity information (**S**) about the L current sources. To make the model more general, the dipole orientation matrix, **A**, is defined:

$$\mathbf{A} = \begin{bmatrix} \mathbf{a}_1 & \mathbf{0} & \cdots & \mathbf{0} \\ \mathbf{0} & \mathbf{a}_2 & \vdots & \vdots \\ \vdots & \cdots & \ddots & \vdots \\ \mathbf{0} & \cdots & \cdots & \mathbf{a}_L \end{bmatrix}_{3L \times L}$$

Where $\mathbf{a}_l = [a_1, a_2, a_3]'$ is the dipole orientation vector for each l unit dipole source generator.

The spatio-temporal model becomes

$$\mathbf{V} = (\mathbf{MA})\mathbf{S} + \mathbf{E} \quad 2.3$$

The transfer matrix **M** in this case is of dimension N by 3L and contains the orthogonal unit components **M_x**, **M_y**, **M_z** for all the dipoles L. Each column of **MA** in equation 2.3 can be viewed as the potential image of a unit dipole on the scalp.

2.1.2 The Principal Component EEG Decomposition

The Principal Component (PC) EEG decomposition is based on the analysis of the covariance matrix of the zero mean recorded potential **V_a** that contains the abnormal features of interest for source localization:

$$\mathbf{R}_a = \mathbf{V}_a \mathbf{V}_a' \quad 2.4$$

The NxN covariance matrix **R_a** is symmetric and positive semidefinite. The elements on the diagonal of **R_a** represent a measure of the variances of the potential variations recorded at each

electrode site n , v_n . The off diagonal elements of \mathbf{R}_a are the covariances between the potential variations recorded at the electrodes. The EEG samples are distributed within some ellipsoidal boundary described by \mathbf{R}_a .

The principal component decomposition of the EEG contains as spatial components a set of orthonormal components. These orthonormal basis vectors are obtained from the covariance matrix through diagonalization. The diagonalization of the covariance matrix results from the eigenvalue-eigenvector decomposition of \mathbf{R}_a . The eigenvectors of the covariance matrix point along the directions of maximum variance in the EEG. This can be demonstrated by applying a transformation of the EEG that results in a signal of maximum variance in the EEG:

$$\tilde{\mathbf{y}} = \tilde{\mathbf{b}}' \mathbf{V}_a \quad 2.5$$

The variance of the signal vector $\tilde{\mathbf{y}}$ is a number that represents the maximum variance and is expressed as

$$\sigma^2 = \tilde{\mathbf{y}} \tilde{\mathbf{y}}' = \tilde{\mathbf{b}}' \mathbf{V}_a \mathbf{V}_a' \tilde{\mathbf{b}} = \tilde{\mathbf{b}}' \mathbf{R}_a \tilde{\mathbf{b}} \quad 2.6$$

The problem becomes the maximization of the last term of equation 2.6 under the constraint that the transformation vector $\tilde{\mathbf{b}}$ is of unit length. The function maximized is

$$F = \tilde{\mathbf{b}}' \mathbf{R}_a \tilde{\mathbf{b}} + \lambda (1 - \tilde{\mathbf{b}}' \tilde{\mathbf{b}}) \quad 2.7$$

The first derivative of the function in 2.7 is calculated:

$$\begin{cases} \frac{\partial F}{\partial \tilde{\mathbf{b}}} = 2(\mathbf{R}_a - \lambda \mathbf{I})\tilde{\mathbf{b}} = \mathbf{0} \\ \frac{\partial F}{\partial \mu} = 1 - \sum_{n=1}^N \tilde{b}_n^2 = 0 \end{cases} \quad 2.8$$

The expressions of the derivatives of F are identified with the eigenvector-eigenvalue problem and indicate that $\tilde{\mathbf{b}}$ and λ are an eigenvector and an eigenvalue respectively of \mathbf{R}_a . By multiplying the left side of the first equation in 2.8 with $\tilde{\mathbf{b}}'$ and substituting equation 2.6,

$$\lambda_{\max} = \frac{\tilde{\mathbf{b}}' \mathbf{R}_a \tilde{\mathbf{b}}}{\tilde{\mathbf{b}}' \tilde{\mathbf{b}}} = \tilde{\mathbf{b}}' \mathbf{R}_a \tilde{\mathbf{b}} = \tilde{\sigma}^2 \quad 2.9$$

Equation 2.9 proves that the eigenvector $\tilde{\mathbf{b}}$, which corresponds to the maximum eigenvalue, points along the direction of maximum variance in the EEG.

It follows that in order that nontrivial solutions $\tilde{\mathbf{b}}$ may exist, λ must be chosen to satisfy the determinant equation

$$|\mathbf{R}_a - \lambda \mathbf{I}| = 0 \quad 2.10$$

This equation is the characteristic equation of the covariance matrix. By solving this equation for λ , the eigenvalues are calculated. Once the eigenvalues are known, the eigenvectors are determined from equations 2.8.

With the notation \mathbf{B} for the eigenvector matrix, with its vector components \mathbf{b} , and $\mathbf{\Lambda}$ for the eigenvalue matrix, with its diagonal components λ , the variances, the relationship between the covariance, eigenvector and the diagonal eigenvalue matrix is

$$\mathbf{R}_a \mathbf{B} = \mathbf{B} \mathbf{\Lambda}$$

Multiplying the left side with \mathbf{B}' and using the property of the orthonormal matrices $\mathbf{B}'\mathbf{B}=\mathbf{I}$ it results that

$$\mathbf{B}'\mathbf{R}_a\mathbf{B} = \mathbf{\Lambda} \quad 2.11$$

A linear transformation that projects the EEG onto the orthonormal basis vectors \mathbf{B} is applied such as:

$$\mathbf{Y} = \mathbf{B}'\mathbf{V}_a \quad 2.12$$

where \mathbf{B}' is the transformation matrix. The covariance of \mathbf{Y} is thus

$$\mathbf{Y}\mathbf{Y}' = \mathbf{B}'\mathbf{V}_a\mathbf{V}_a'\mathbf{B} = \mathbf{B}'\mathbf{R}_a\mathbf{B} = \mathbf{\Lambda} \quad 2.13$$

The relationship between this covariance matrix and the diagonal eigenvalue matrix demonstrates that the linear transformation results in a set of uncorrelated waveforms \mathbf{Y} . The eigenvalue matrix contains, in decreasing order, the amount of the variance that each waveform accounts for in the measured EEG.

The EEG can be then expressed as

$$\mathbf{V}_a = \mathbf{B}\mathbf{Y} \quad 2.14$$

This is the Principal Component spatio-temporal decomposition of the EEG. The columns of \mathbf{B} contain the PC spatial patterns and the rows of \mathbf{Y} the corresponding temporal patterns.

The EEG samples are distributed within some ellipsoidal boundary of radii λ , in the directions of the corresponding columns in \mathbf{B} . The diagonal square matrix Λ combines both the signal and noise eigenvalues (variances) of \mathbf{V}_a and can be partitioned into two submatrices Λ_s and Λ_e where Λ_e contains the zero or close to zero eigenvalues. The number of zero eigenvalues is $N - \text{rank}(\mathbf{R}_a)$. The eigenvalues are in decreasing order and consequently Λ_s contains the first eigenvalues significantly greater than 0. The set of corresponding eigenvectors \mathbf{B}_s are estimated as the spatial pattern components that point in the direction of significantly high variance in \mathbf{V}_a , spanning the signal subspace (of interest). The rest of columns in \mathbf{B} , \mathbf{B}_e , span the complement (*Halmos*, 1974) of the signal subspace, the noise subspace. The PC decomposition can be then expressed as

$$\mathbf{V}_a = [\mathbf{B}_s \ \mathbf{B}_e] \begin{bmatrix} \mathbf{Y}_s \\ \mathbf{Y}_e \end{bmatrix} \quad 2.15$$

and the covariance matrix

$$\mathbf{R}_a = [\mathbf{B}_s \ \mathbf{B}_e] \begin{bmatrix} \Lambda_s & \mathbf{0} \\ \mathbf{0} & \Lambda_e \end{bmatrix} [\mathbf{B}_s \ \mathbf{B}_e]^T \quad 2.16$$

2.1.3 *The Common Spatial Pattern Decomposition*

In the previous section the Principal Component method of decomposing an abnormal segment of the EEG was presented. The PC decomposition is based on a set of orthonormal spatial components and their orthogonal temporal components. Each component contains, besides the abnormal signal of interest, background components from various normal neural activity and additive noise. The filtering of the noise and the normal patterns would result in a

better indication of the true location of the abnormal sources. The method of Common Spatial Pattern Decomposition, that was described by *Koles* in 1991, may result in a more distinctive separation of the EEG into components that have more clinical relevance, as it appears to enable individual sources to be better isolated (*Koles et al.*, 1995).

This method necessitates two sets of data, one before the seizure- the normal EEG, or EEG_n (V_n), and one containing the abnormal patterns-EEG_a (V_a). The CSP method is based on PC analysis but the spatial components are not constrained to be orthonormal or even orthogonal, but constrained to account for maximally different proportions of the total variance present in the abnormal and normal EEGs. In other words, the spatial patterns point in the directions of maximum differences in variance between the two EEGs.

Common spatial pattern decomposition is performed starting with the calculation of the sum covariance matrix, R :

$$R = R_a + R_n \quad 2.17$$

where R_a is the covariance matrix of the abnormal EEG, and R_n is the covariance matrix of the normal EEG. The covariance matrix R is decomposed into eigenvalues and eigenvectors as before:

$$R = B_c \Lambda_c B_c' \quad 2.18$$

A transformation matrix is applied to the data, which makes the covariance matrix equal to I , by changing the scales of the principal components in proportion of $\Lambda_c^{-1/2}$. This whitening transformation is applied to both EEGs (normal and abnormal).

$$\mathbf{P} = \Lambda_c^{-1/2} \mathbf{B}_c' \quad 2.19$$

Since Λ_c is a square diagonal matrix, with element values in decreasing order, possibly with some equal to zero, it may be necessary to reduce its dimension in order to apply the inverse $\Lambda_c^{-1/2}$, which results in a diagonal matrix with its elements $1/\lambda^{1/2}$. In the whitened space, the EEG samples are distributed within a unit radius spheroidal boundary. This can be demonstrated by calculating the covariance matrix of the whitened data. The whitening transformation is applied to the covariance matrices, \mathbf{R}_a and \mathbf{R}_n individually:

$$\begin{aligned} \mathbf{S}_a &= \mathbf{P} \mathbf{R}_a \mathbf{P}' \\ \mathbf{S}_n &= \mathbf{P} \mathbf{R}_n \mathbf{P}' \end{aligned} \quad 2.20$$

It can be shown (*Fukunaga*, 1972) that the whitened covariance matrices above share the same eigenvectors (common spatial patterns):

$$\begin{aligned} \mathbf{S}_a &= \mathbf{U} \Psi_a \mathbf{U}' \\ \mathbf{S}_n &= \mathbf{U} \Psi_n \mathbf{U}' \end{aligned} \quad 2.21$$

with

$$\Psi_a + \Psi_n = \mathbf{I} \quad 2.22$$

The last result is very important for the separation of the EEG_a and EEG_n. In the whitened measurement space spanned by \mathbf{U} , the variance accounted for by the first eigenvectors (those corresponding to the largest eigenvalues in Ψ_a) will be maximal for EEG_a. Because of the sum constraint on Ψ_n , the variance accounted for by these eigenvectors must

be then minimal for EEG_n. The reverse is also true for the remaining eigenvectors (for which the eigenvalues in Ψ_n are maximal). Therefore, a transformation of the EEG epochs by $\mathbf{P}'\mathbf{U}$ will yield a decomposition that is optimal for separating the variances in the two EEGs. As with PC, the application of this spatial filter to an EEG data matrix will extract a set of temporal waveforms that meet this variance constraint. The linear transformation can be written:

$$\mathbf{Z} = (\mathbf{P}'\mathbf{U})' \mathbf{V} \quad 2.23$$

where \mathbf{Z} is the set of waveforms, both the abnormal and normal temporal patterns present in \mathbf{V} . It follows that the covariance of the temporal patterns present in EEG_a, \mathbf{Z}_a is

$$\mathbf{Z}_a \mathbf{Z}_a' = [(\mathbf{P}'\mathbf{U})' \mathbf{V}_a] [(\mathbf{P}'\mathbf{U})' \mathbf{V}_a]' = \mathbf{U}' \mathbf{P} \mathbf{R}_a \mathbf{P}' \mathbf{U} = \mathbf{U}' \mathbf{S}_a \mathbf{U} = \Psi_a \quad 2.24$$

and that the rows of \mathbf{Z}_a are uncorrelated. Only the temporal patterns in \mathbf{Z} that correspond to greater eigenvalues in Ψ_a than in Ψ_n are thought of as being generated by abnormal signal sources. The set of the corresponding common spatial patterns is calculated as follows:

$$\mathbf{C} = (\mathbf{U}'\mathbf{P})^* \quad 2.25$$

where \mathbf{C} can have any of the dimensions $N \times (\leq N)$ and $(.)^*$ is the pseudoinverse. The abnormal EEG can then be expressed as:

$$\mathbf{V}_a = \mathbf{C} \mathbf{Z}_a \quad 2.26$$

This is the Common Spatial Pattern decomposition of the EEG. From the set of column vectors \mathbf{C} , only the spatial patterns that correspond to the abnormal sources are retained. These vectors, \mathbf{C}_s , that span the signal space, point in the direction of maximum variance in the abnormal EEG (first significant eigenvalues in Ψ_a, Ψ_{a_c}), and minimum variance in the normal EEG, thus maximum difference $(\psi_a - \psi_n)$, where ψ are the eigenvalues. This is used as a criterion in separating the abnormal spatial components of interest from the normal spatial components. It follows that, the rest of the spatial components, \mathbf{C}_e , which account for minimum variance in the abnormal EEG and maximum variance in the normal EEG (zero or close to zero diagonal elements in Ψ_a, Ψ_{a_c}) span the noise space. The waveforms in \mathbf{Z} of maximum variance in the abnormal EEG are considered to be closest to the abnormal temporal patterns of interest. The CSP decomposition of the abnormal EEG \mathbf{V}_a can then be also written as

$$\mathbf{V}_a = \mathbf{C}_s \mathbf{Z}_{a_s} + \mathbf{C}_e \mathbf{Z}_{a_e} \quad 2.27$$

and using the result from the equation 2.24 and the previous considerations, the scaled covariance matrix can be expressed as

$$\mathbf{V}_a \mathbf{V}_a' = \mathbf{C}_s \Psi_a \mathbf{C}_s' + \mathbf{C}_e \Psi_{a_e} \mathbf{C}_e' \quad 2.28$$

It can be remarked that the sets of equations 2.27 - 2.28 and 2.15 - 2.16 are of similar form.

2.2 Source Localization Methods

For the available measured EEG, \mathbf{V} , the source localization procedure involves finding the appropriate set of \mathbf{M} (locations), \mathbf{S} (dipole moments) and orientations \mathbf{A} that produce \mathbf{V} . This

is known as the inverse problem in EEG. In the next three subchapters three methods of determining primarily the spatial information, which means the location of the sources in the head, and, where necessary, the temporal and orientation information will be described.

2.2.1 *Single Dipole Fitting*

The spatio-temporal model of the EEG, equation 2.3, requires that L , the number of sources, their locations, orientations and moments, be known beforehand. In practice only the measured EEG (\mathbf{V}) and the unit dipole model calculated at each grid point in the head model are known. For the unit dipole model at any grid point the notation $\hat{\mathbf{M}}$ is used.

The Single Dipole Fitting source localization method involves the scanning of all of the grid points in the head model for which the $N \times 3$ transfer matrix $\hat{\mathbf{M}}$, containing the three orthogonal unit components $\hat{\mathbf{M}}_x$, $\hat{\mathbf{M}}_y$, $\hat{\mathbf{M}}_z$, has been pre-computed and finding the best fit of this candidate source to the measured data \mathbf{V} .

Since the transfer matrix $\hat{\mathbf{M}}$ is of full column rank 3, smaller than the measurement sites N , this is an overdetermined problem. This means that there are more equations than unknowns. Grouping the orientation matrix with the dipole moment matrix and letting $\hat{\mathbf{A}}$ and $\hat{\mathbf{S}}$ be the set of estimates of the source orientation and magnitude, the error function

$$\bar{J}_1 = \left\| \mathbf{V} - \hat{\mathbf{M}}(\hat{\mathbf{A}}\hat{\mathbf{S}}) \right\|_F^2 \quad 2.29$$

is minimized with respect to $\hat{\mathbf{A}}\hat{\mathbf{S}}$. $\|\cdot\|_F$ is the Frobenius norm, or matrix norm, and $\|\cdot\|_F^2$ in this case represents the squared error between the measured data and the EEG model.

The least-squares approximation, $\hat{\mathbf{A}}\hat{\mathbf{S}}$, based on the T data points, that minimizes the error function J_1 at each grid point can be expressed in terms of the pseudoinverse $\hat{\mathbf{M}}^*$ (Penrose, 1955, Brogan, 1991) as

$$\hat{\mathbf{A}}\hat{\mathbf{S}} = \hat{\mathbf{M}}^* \mathbf{V} \quad 2.30$$

where

$$\hat{\mathbf{M}}^* = (\hat{\mathbf{M}}\hat{\mathbf{M}})^{-1} \hat{\mathbf{M}} \quad 2.31$$

is the pseudoinverse of the nonsquare matrix $\hat{\mathbf{M}}$, since $\hat{\mathbf{M}}$ has linearly independent columns and consequently $\hat{\mathbf{M}}\hat{\mathbf{M}}$ is of full rank 3. $\hat{\mathbf{M}}^*$ has the properties

$$\hat{\mathbf{M}}^*\hat{\mathbf{M}} = \mathbf{I} \text{ and } \hat{\mathbf{M}}\hat{\mathbf{M}}^* \neq \mathbf{I} \quad 2.32$$

$\hat{\mathbf{A}}\hat{\mathbf{S}}$ is the approximate solution to the overdetermined least square problem and the amount of error in this approximate solution is indicated by J_1 . Substituting the linear terms $\hat{\mathbf{A}}\hat{\mathbf{S}}$ from equation 2.30 into 2.29, the error function formula becomes

$$\bar{J}_1 = \left\| (\mathbf{I} - \hat{\mathbf{M}}\hat{\mathbf{M}}^*) \mathbf{V} \right\|_F^2 \quad 2.33$$

In this formula, the data is projected onto the left null space (Strang, 1980) of the candidate source at each grid point. The formula yields a number which represents the accumulated least square error over all of the time points T. The scanning of the head means in fact calculating

this error at all of the grid points and retaining the grid point location for which the error is minimum.

If the data \mathbf{V} is decomposed using the Principal Component Decomposition, equation 2.14, it can be easily demonstrated using the definition of the Frobenius norm and the property of the orthogonal matrix \mathbf{Y} (equation 2.13) that the value of J_1 is preserved for $\mathbf{V}=\mathbf{B}\mathbf{\Lambda}$. J_1 can be then written as

$$\bar{J}_1 = \left\| (\mathbf{I} - \hat{\mathbf{M}}\hat{\mathbf{M}}^*) \mathbf{B}\mathbf{\Lambda} \right\|_F^2 \quad 2.34$$

Using $\mathbf{B}\mathbf{\Lambda}$ in the minimization function J_1 has the advantage of reducing the computational cost of the matrix norm. Rather than calculating the sum of the squares of the projection of a $N \times T$ matrix, \mathbf{V} , on the left null projector of $\hat{\mathbf{M}}$, the norm of a maximum $N \times N$ matrix is now to be calculated. The number of columns of the matrix $(\mathbf{I} - \hat{\mathbf{M}}\hat{\mathbf{M}}^*) \mathbf{B}\mathbf{\Lambda}$ is equal to the $\text{rank}(\mathbf{B})$ and is also equal to the number of nonzero singular values in $\mathbf{\Lambda}$. In practice, however, the signal space and the noise space are estimated as presented in Chapter 2.1.2, based on the decision of which eigenvalues are close enough to zero. The noise spatial and temporal components are separated from the signal components (equations 2.15, 2.16) and filtered out. The function reduces to

$$J_1 = \left\| (\mathbf{I} - \hat{\mathbf{M}}\hat{\mathbf{M}}^*) \mathbf{B}_s \mathbf{\Lambda}_s \right\|_F^2 \quad 2.35$$

The potential \mathbf{V} has smaller values if produced by deep sources than if produced by superficial sources. Due to the fact that the calculation of the head model is based on the

assumption that the head is purely conductive, the unit dipole model for the deep sources is described by small transfer coefficients. For these reasons, J_1 is scaled such that it is not a function of small transfer coefficients or/and small recorded potentials. In other words, it does not depend on depth. Then the minimum will indicate the closeness to orthogonality between the columns in $\mathbf{B}_s\Lambda_s$ and the null space of $\hat{\mathbf{M}}$. It is noted that the value of J_1 will be 0 for the case of a perfect fit between the model and the data.

To plot the scaled cost function calculated at each grid point so that the minima at the determined source locations can be displayed as maxima, the negative of the logarithmic scale is used. For each grid point a measure called the Source Location Index (SLI_1) is defined as:

$$SLI_1(x, y, z) = -\lg \frac{J_{1\min}(x, y, z)}{\|\hat{\mathbf{M}}\hat{\mathbf{M}}^*\mathbf{B}_s\Lambda_s\|_F^2} \quad 2.36$$

Now, the value of the source location index approaches infinity at the grid points where the minimum of J_1 approaches zero.

In order to quantify estimated source locations, the Goodness Of Fit (GOF) is defined:

$$GOF(\%) = \left(1 - \frac{\|(\mathbf{I} - \hat{\mathbf{M}}\hat{\mathbf{M}}^*)\mathbf{B}_s\Lambda_s\|_F^2}{\|\hat{\mathbf{M}}\hat{\mathbf{M}}^*\mathbf{B}_s\Lambda_s\|_F^2} \right) \times 100 \quad 2.37$$

The squared norms in the denominators of equations 2.36 and 2.37 represent the square error between the data $\mathbf{V}(t)$ and the estimate $\hat{\mathbf{M}}(\hat{\mathbf{A}}\hat{\mathbf{S}})$. The squared relative error is the ratio of

the two norms and can be identified with the argument of the logarithmic function of the source location index.

The aim is to find a value for SLI_1 that would result in a good fit between the model and the data. Based on the previous results

$$1 - GOF = \frac{J_{\min}(x, y, x)}{\|\hat{\mathbf{M}}\hat{\mathbf{M}}^* \mathbf{B}_s \Lambda_s\|_F^2} \quad 2.38$$

It is assumed that a good fit corresponds to an error smaller than 0.01 which means that the data explains the model at least within 99%. That is, $GOF \geq 0.99$ and using the notation for the logarithmic function $\lg = \log_{10} \Rightarrow -\lg(1 - 0.99) = SLI_1 \geq 2$. Then the decision for the peaks that correspond to dipole locations is made based on the values of the SLI_1 which must be at least 2 in order to obtain a good fit.

It can be easily observed that for $GOF=100\%$ the estimate $\hat{\mathbf{M}}(\hat{\mathbf{A}}\hat{\mathbf{S}})$ perfectly fits the data \mathbf{V} , the columns of $\mathbf{B}_s \Lambda_s$ are orthogonal to the left null space of $\hat{\mathbf{M}}$, that is all of the error expressions are 0 and the SLI_1 is ∞ . This can be obtained in simulations but is not likely to be the case with real data. Since only one dipole model is used for fitting the data, only data that will be fully explained by one dipole source will be correctly localized.

The method of single dipole fitting can be applied to multiple sources as well. If instead of one unit dipole model $\hat{\mathbf{M}}$ a set of dipole models is used in the minimization function this minimization process results in successively scanning the head with only one dipole, the others being kept fixed. The source location index is maximum at all of the locations where the set of

$\hat{\mathbf{M}}\mathbf{s}$ gives a good approximation to $\mathbf{B}_s\mathbf{A}_s$. The disadvantage of this method is that the pseudoinverse of a larger model matrix has to be pre-computed and stored.

2.2.2 Multiple Dipole Fitting

A more economical approach to localizing multiple dipoles is the Multiple Signal Classification (MUSIC) method. The MUSIC algorithm was first developed by Schmidt in 1979 and applied in Source Localization by Mosher et al., 1992. The algorithm is used to calculate, at each grid point, the minimum projection of an optimal linear combination of the columns of $\hat{\mathbf{M}}$ on the noise subspace spanned by a set of eigenvectors.

In this work, the MUSIC algorithm is modified so that the CSP decomposition of the EEG presented in Chapter 2.1.3 can be used for the noise projector matrix. The noise subspace is considered to be spanned by the CSPs \mathbf{C}_e that account for minimum variance in the abnormal EEG, therefore correspond to the smallest eigenvalues in Ψ_a , as shown before. The noise subspace is the left null space of the CSPs, \mathbf{C}_s , that span the signal subspace. Ideally, the vectors that span the signal subspace will be orthogonal to the vectors that span the noise subspace. The two summed subspaces form the measurement space.

The MUSIC method is based on three assumptions, as stated by Mosher et al. One assumption is that the transfer matrix is full column rank. Another assumption is that the noise is white, with zero mean and variance σ^2 . The other is that the moment time series for different dipole components are not correlated. The first two assumptions were stated in Chapter 2.1.1. The last assumption means that the rows of matrix \mathbf{S} from the forward EEG model are linearly independent, thus no current source can be expressed as a linear combination of the others, in other words, the current sources of the dipoles are uncorrelated.

The implementation of the MUSIC algorithm in the present method involves minimizing the error between a linear combination of the CSPs, \mathbf{C}_s , spanning the abnormal EEG signal space, and the same number of sources $\mathbf{M}_a \mathbf{A}_a$. Mathematically this can be expressed as

$$\bar{J}_2 = \|\mathbf{M}_a \mathbf{A}_a - \mathbf{C}_s \mathfrak{R}\|_F^2 \quad 2.39$$

This error is minimum when

$$\mathfrak{R} = \mathbf{C}_s^* \mathbf{M}_a \mathbf{A}_a \quad 2.40$$

Substituting 2.40 in 2.39 \bar{J}_2 results in

$$\bar{J}_2 = \left\| (\mathbf{I} - \mathbf{C}_s \mathbf{C}_s^*) \mathbf{M}_a \mathbf{A}_a \right\|_F^2 \quad 2.41$$

Equation 2.41 indicates that \bar{J}_2 is the sum of the projections of the columns of $\mathbf{M}_a \mathbf{A}_a$ on the left null space of the spatial components \mathbf{C}_s . This means that minima of J_2 can be found at some L grid points by scanning all of the head volume with a single dipole source described by $\hat{\mathbf{M}} \mathbf{a}$, where \mathbf{a} is an estimate of \mathbf{a} . Consequently, in order to determine the best linear combination of the columns of $\hat{\mathbf{M}}$ that project on the left null space of the signal vectors and result in a minimum at each grid point, the alternative minimization function is used:

$$J_2 = \left\| (\mathbf{I} - \mathbf{C}_s \mathbf{C}_s^*) \hat{\mathbf{M}} \mathbf{a} \right\|_F^2 \quad 2.42$$

$$\text{Let } \Phi = (\mathbf{I} - \mathbf{C}_s \mathbf{C}_s^*) \hat{\mathbf{M}} \quad 2.43$$

The projection matrix $(\mathbf{I} - \mathbf{C}_s \mathbf{C}_s^*)$ can be pre-computed and the images of the candidate source $\hat{\mathbf{M}}$ at each grid point are also known from the head model. Hence, the matrix norm J_2 can be expressed as:

$$J_2 = \mathbf{a}' \Phi' \Phi \mathbf{a} = \mathbf{a}' \Sigma \mathbf{a} \quad 2.44$$

where the matrix Φ is of dimension $N \times 3$ and Σ is symmetric and of dimension 3×3 .

The equation above suggests that at every grid point, for the known Φ , some unit dipole orientation vector \mathbf{a} can be found such that J_2 is minimum. The minimization function that incorporates this constraint is

$$H = J_2 + \lambda(1 - \|\mathbf{a}\|_2^2) \quad 2.45$$

where λ is the Lagrange multiplier.

Substituting J_2 from 2.44, 2.45 becomes

$$H = \mathbf{a}' \Sigma \mathbf{a} + \lambda(1 - \mathbf{a}' \mathbf{a})$$

In order to find the minimum of this function, the first derivative of H is calculated:

$$\begin{cases} \frac{\partial H}{\partial \mathbf{a}} = 2(\Sigma - \lambda \mathbf{I}) \mathbf{a} = \mathbf{0} \\ \frac{\partial H}{\partial \lambda} = 1 - (a_1^2 + a_2^2 + a_3^2) = 0 \end{cases} \quad 2.46$$

and hence \mathbf{a} and λ are eigenvectors and eigenvalues of Σ respectively . Multiplying the left side of the first equation above with \mathbf{a}' , the minimum of the function J_2 is

$$J_{2\min} = \frac{\hat{\mathbf{a}}' \Sigma \hat{\mathbf{a}}}{\hat{\mathbf{a}}' \hat{\mathbf{a}}} = \lambda_{\min} \quad 2.47$$

The eigenvector $\hat{\mathbf{a}}$ is the best orientation of the dipole at a specific location that minimizes J_2 , and therefore this eigenvector corresponds to the minimum of the eigenvalues resulting from solving the system of equations 2.46. Therefore, to determine $J_{2\min}$ it is sufficient to calculate the eigenvalues and eigenvectors of the 3x3 matrix Σ , and retain the eigenvector corresponding to the minimum eigenvalue.

To eliminate the bias on source localization due to $\hat{\mathbf{M}}$,

$$\hat{\mathbf{m}}_a = \hat{\mathbf{M}} \hat{\mathbf{a}} \quad 2.48$$

is introduced. $\hat{\mathbf{m}}_a$ is the optimum linear combination of the columns of $\hat{\mathbf{M}}$ that minimizes its projection on the left null space of the signal components \mathbf{C}_s over all possible orientations. The minimum of J_2 scaled with the norm of $\hat{\mathbf{m}}_a$ yields

$$\frac{J_{2\min}}{\|\hat{\mathbf{m}}_a\|_2^2} = \frac{\|(\mathbf{I} - \mathbf{C}_s \mathbf{C}_s') \hat{\mathbf{m}}_a\|_2^2}{\|\hat{\mathbf{m}}_a\|_2^2} = \frac{\lambda_{\min}}{\|\hat{\mathbf{m}}_a\|_2^2} \quad 2.49$$

To display the scaled $J_{2\min}$ at locations (x,y,z) , the SLI_2 is defined as:

$$SLI_2(x, y, z) = -\lg \frac{J_{2\min}(x, y, z)}{\|\hat{\mathbf{m}}_a\|_2^2} \quad 2.50$$

$SLI_2(x, y, z)$ will show peaks at the grid points where J_2 is minimum.

Similar to the case of Single Dipole Fitting, the goodness of fit is defined as follows:

$$GOF_2(\%) = \left(1 - \frac{\|(\mathbf{I} - \mathbf{C}_s \mathbf{C}_s^*) \hat{\mathbf{m}}_a\|_2^2}{\|\hat{\mathbf{m}}_a\|_2^2} \right) \times 100 = \left(1 - \frac{\lambda_{\min}}{\|\hat{\mathbf{m}}_a\|_2^2} \right) \times 100 \quad 2.51$$

If the admissible range for the GOF_2 is set to be greater than 99%, the SLI_2 is greater than 2. Therefore, any peak greater than this value will be considered a true dipole location. For a GOF_2 approaching 100%, $\hat{\mathbf{m}}_a$ is closely orthogonal on the left null space of \mathbf{C}_s , the error is close to zero and the SLI_2 tends to infinity.

2.2.3 LORETA

The two previous methods of localizing the sources of the EEG assume that the sources are current dipoles. They involve the scanning of the head with a candidate source and finding the best fit between this source model and some estimated spatial components, derived from the data, spanning the signal space. In practice, it is more likely that the sources that are assumed to be dipoles are actually distributed dipole sheets with some shape determined by the neuronal anatomy. These neighboring neurons are likely to be synchronously active and as a result the sources within the dipole sheet are correlated. The previous methods would then localize an equivalent dipole. If the data were produced by synchronous neuronal activity over a broader volume conductor, both preceding localization procedures based on dipole fitting would fail to correctly describe the spatial origin of the electrical activity. *Mosher et al.*, 1998,

describe an extension of the MUSIC algorithm, R-MUSIC, based on the correlation between the dipole model and the signal subspace, which, in simulations, localizes correlated sources.

A method of localizing sources of EEG without the requirement that the source model be a current dipole, or that the sources be asynchronous, is the minimum norm. The minimum norm estimates the current density over all grid points in the head model, with the locations for the true sources being in the regions where the density is maximum. This only requires knowledge about the head model and the measured data. The head model matrix contains the transfer matrices $\hat{\mathbf{M}}$ for all of the grid points and uses the composite matrix $\tilde{\mathbf{M}}$ of dimension $N \times 3G$, with G the number of grid points. The matrix $\tilde{\mathbf{M}}$ will result in a number of columns at least of the order of thousands even for a very coarse grid. For one time slice, the moments are related to the measured potentials by the expression

$$\mathbf{v} = \tilde{\mathbf{M}}\mathbf{i} \tag{2.52}$$

where \mathbf{i} is the current density vector comprised of the i_x, i_y, i_z components for the G grid points. The dimension of \mathbf{i} is therefore $3G \times 1$. The objective is to determine \mathbf{i} that leads to \mathbf{v} . The problem is that the system of N equations has $3G$ unknowns and this is a highly underdetermined problem, hence with an infinite number of solutions for \mathbf{i} .

Researchers have followed several approaches in the attempt to find a unique solution for \mathbf{i} (Gorodnitsky et al., 1995, Srebro, 1996). The minimum norm solution is

$$\mathbf{i} = \tilde{\mathbf{M}}^* \mathbf{v} \tag{2.53}$$

It has been shown that this solution is biased towards the surface. In order to obtain the unbiased minimum norm solution a diagonal weighting matrix is constructed and the solution becomes a weighted minimum norm solution.

Srebro normalizes the columns of $\tilde{\mathbf{M}}$, finds the solution $\mathbf{i} = \mathbf{W}\tilde{\mathbf{M}}^* \mathbf{v}$, where \mathbf{W} is a diagonal matrix containing the norm of all columns of $\tilde{\mathbf{M}}$, and calculates the solution through iteratively imposing regularization constraints by separating a smaller group of grid points that have larger values i of \mathbf{i} . *Gorodnitsky* uses an iterative algorithm where the diagonal elements in the weighting matrix are at each iteration the ratio between the elements of the solution obtained from the previous iteration step and the norm of the corresponding column of $\tilde{\mathbf{M}}$. This way, the estimated initial solution, with currents dispersed over a large area in the brain, is sharpened such as only some of the elements i are nonzero while the rest of the elements are decreased until they become zero. It is shown that the method works remarkably well in simulations for single sources and, with some constraints, also for distributed sources.

A method called LORETA (Low Resolution Electromagnetic Tomography), that directly computes the smoothest 3D distribution of the current density in the head volume, was developed by *Pascual-Marqui, et al.* in 1994. The main appeal of LORETA is that it directly calculates the generalized inverse of $\tilde{\mathbf{M}}$ as a unique linear transformation of \mathbf{v} into \mathbf{i} . The solution is a minimum norm restricted solution, developed in the cited work for single time slices.

In this work, the LORETA is extended to multiple time slice minimum norm source localization. The LORETA solution is used with the CSP decomposition of the abnormal EEG in order to determine the current density over all of the grid points of the 3D volume of

the head. However, any EEG decomposition can be used in order to find the solution. That is, the LORETA solution is the smoothest possible source current density distribution, which can account for the measurements on the scalp. This can be expressed as

$$J_3 = \min_i \|\mathbf{L}\mathbf{W}\mathbf{i}\|_2^2 \quad 2.54$$

under the constraint $\mathbf{v} = \tilde{\mathbf{M}}\mathbf{i}$, where \mathbf{i} is the current density vector, \mathbf{W} is the weighting matrix as described above, and \mathbf{L} is the $3G \times 3G$ laplacian matrix. The transfer matrix $\tilde{\mathbf{M}}$ has linearly independent columns.

The multiple time slice source localization proposed in this work, based on the solution for a single time slice, as in LORETA, is performed in three steps:

1. The matrices \mathbf{W} and \mathbf{L} are calculated. The matrix \mathbf{W} is of form

$$\mathbf{W} = \text{diag}(\|\tilde{\mathbf{m}}_k\|_2), \quad \text{with } k = \overline{1, 3G} \quad 2.55$$

The diagonal weighting matrix \mathbf{W} is of rank $3G$. The laplacian of the weighted \mathbf{i} is equal to the 3D discrete laplacian operator calculated for the regular cubic grid (with G points of coordinates (x, y, z) multiplied by the weighted \mathbf{i} . \mathbf{L} is then formed such that for each grid point the three coordinates are assigned the number 6, whereas the neighbours placed at the minimum distance, d , between grid points are assigned the number -1 . This rule is applied irrespective to the number of neighbors, that is at the edges as well as within the volume. All of the elements are divided by the square distance, d^2 , between grid points on any of the direction x , y , or z . This is consistent with the formula for the sharpened weighted current density at each grid point, g , given by *Pascual-Marqui et al.*:

$$\mathbf{l}_g = \frac{1}{d^2} \left(6\rho_g - \sum_p \rho_p \right), \forall p \text{ such as } d = \|\vec{r}_g - \vec{r}_p\| \quad 2.56$$

where r is the position vector of the grid points p and g , ρ being the weighted current density at the grid points. The laplacian matrix \mathbf{L} is symmetric ($\mathbf{L}\mathbf{L} = \mathbf{L}^2$), multidiagonal, sparse, and positive definite. The nonsingularity is due to the fact that at the edges the values for the grid points and their neighbors are kept the same as in the rest of the volume, irrespective to the number of neighbours. As a result of symmetry the matrix $\mathbf{W}\mathbf{L}\mathbf{L}\mathbf{W}$ becomes $\mathbf{W}\mathbf{L}^2\mathbf{W}$. This matrix is symmetric and positive definite.

2. It can be shown (Rao et al, 1973), that from the class of all restricted solutions,

the solution that has the least norm $\|\mathbf{i}\|_2$ is obtained by calculating the restricted minimum $\mathbf{W}\mathbf{L}^2\mathbf{W}$ norm generalized-inverse of $\tilde{\mathbf{M}}$. For the problem presented in this work, the formula for this inverse is an adapted form of the formula given by Pascual- Marqui et al. for LORETA, and is written as

$$\mathbf{T} = (\mathbf{W}\mathbf{L}^2\mathbf{W})^{-1} \tilde{\mathbf{M}} \left[\tilde{\mathbf{M}} (\mathbf{W}\mathbf{L}^2\mathbf{W})^{-1} \tilde{\mathbf{M}} \right]^{-1} \quad 2.57$$

The LORETA transformation matrix \mathbf{T} , of dimension $3G \times N$, is thus calculated using only the inverses of square matrices. The only challenge that the computation of \mathbf{T} may bring is due to the great dimension of the matrix $\mathbf{W}\mathbf{L}^2\mathbf{W}$. Constraining the grid to the cortical regions is one possible solution to this problem. The smoothest current density that explains \mathbf{v} is the unique, restricted solution of 2.52:

$$\hat{\mathbf{i}} = \mathbf{T}\mathbf{v} \quad 2.58$$

as in LORETA. Making the notation

$$\bar{\mathbf{M}} = \tilde{\mathbf{M}}(\mathbf{W}\mathbf{L}^2\mathbf{W})^{-1} \quad 2.59$$

the following equalities can be derived:

$$\mathbf{v} = \mathbf{T}^*\hat{\mathbf{i}} = \bar{\mathbf{M}}(\mathbf{W}\mathbf{L}^2\mathbf{W})\hat{\mathbf{i}} = (\tilde{\mathbf{M}}\mathbf{W}^{-1})(\mathbf{W}\hat{\mathbf{i}}) = \tilde{\mathbf{M}}\hat{\mathbf{i}} \quad 2.60$$

This series of equalities is important from three reasons:

- The equality between \mathbf{v} and the last term, derived as shown, demonstrates that the restricted solution explains the data.
- The equality between the second and the last term proves that \mathbf{T} , expressed as in equation 2.57, is a restricted minimum norm generalized inverse of $\tilde{\mathbf{M}}$, as defined in Rao et. al., 1973 (p. 481, case 6).
- The equality between \mathbf{v} and the fourth term shows that \mathbf{v} is expressed in terms of the normalized basis function $\tilde{\mathbf{M}}\mathbf{W}^{-1}$. That is, the current densities at all of the grid points are given equal weight regardless the depth.

3. Once the LORETA transfer matrix \mathbf{T} is computed, the solution for multiple time slices is written:

$$\hat{\mathbf{I}} = \mathbf{T}\mathbf{V} \quad 2.61$$

In this equation, \mathbf{V} is the $N \times T$ measured electric potential and $\hat{\mathbf{I}}$ is a $3G \times T$ current density matrix. In order to localize the abnormal sources, the proposed method is to determine, for each grid point, the variance of the current density using the CSP decomposition of the abnormal EEG, \mathbf{V}_a . The variance of the components on the coordinates x, y, z of the current density at all grid points is contained in the diagonal of the current density covariance matrix:

$$\mathbf{i}_a = \text{diag}(\hat{\mathbf{I}}_a \hat{\mathbf{I}}_a') \quad 2.62$$

where $\hat{\mathbf{I}}_a = \mathbf{T}\mathbf{V}_a$. If \mathbf{V}_a is substituted from equation 2.26, the result in 2.62 becomes,

$$\mathbf{i}_a = \text{diag}(\mathbf{T}\mathbf{V}_a \mathbf{V}_a' \mathbf{T}') = \text{diag}(\mathbf{T}\mathbf{C}\mathbf{Z}_a \mathbf{Z}_a' \mathbf{C}' \mathbf{T}') = \text{diag}(\mathbf{T}\mathbf{C}_a \Psi_a \mathbf{C}_a' \mathbf{T}') \quad 2.63$$

It is noted that the term $\mathbf{V}_a \mathbf{V}_a'$ is the scaled covariance matrix of the abnormal EEG, expressed here in terms of the CSP decomposition 2.26. Since the aim is to localize only the sources responsible for the abnormal activity present in the abnormal EEG and filter out any normal activity and noise from the results in equation 2.28 and 2.63 it follows that the variance of the current density of interest is

$$\mathbf{i}_s = \text{diag}(\mathbf{T}\mathbf{C}_s \Psi_a \mathbf{C}_s' \mathbf{T}') \quad 2.64$$

The total variance of the current density at one grid point g is the sum of the variances of the components on the coordinates x, y, z

$$\mathbf{i}_g(x, y, z) = \mathbf{i}_g(x) + \mathbf{i}_g(y) + \mathbf{i}_g(z) \quad 2.65$$

2.3 Seizure onset (temporal) localization

One of the main challenges in epileptic source localization is the temporal localization of the seizure onset, which is determining the temporal boundary between the normal and abnormal EEG segments. In this work, the seizure onset is detected using a band pass filter, of the CSP decomposition and the MUSIC algorithm. In short, the whole recorded EEG \mathbf{V} is successively band pass and spatially filtered and the SLI_2 calculated. The choice for the band pass filter and the normal and abnormal epochs is made based on the maximum of all SLI_2 , greater than 2, obtainable.

3 SIMULATION RESULTS

This chapter presents simulation results that illustrate the spatio-temporal decomposition and the source localization methods described in the previous section, applied to a simulated EEG.

3.1 EEG Spatio-Temporal Decompositions

An EEG is first simulated applying the spatio-temporal model and then decomposed using the Principal Component decomposition and the Common Spatial Pattern decomposition. For each decomposition the spatial and temporal components are plotted such that they can be compared to the spatio-temporal model.

3.1.1 *The EEG Model*

The EEG is simulated at 25 electrodes using the spatio-temporal model in equation 2.3, with no additive noise ($\mathbf{E}=0$), for the case of three ($L=3$) uncorrelated sources which, for illustrative purposes, are located in the same plane, $y=0$, shown in Figure 3.1. The electrode positions are at the same angles as in Figure 1.1 on a sphere of unit radius, which represents the outer boundary of the scalp in the three-shell head model. The two inner circles, of radii 0.87 and 0.92 delimit the skull. The electrodes positioned on the outer circle in the $y=0$ plane are shown in Figure 3.1a: T3, C3, Cz, C4, T4, from left to right. The potentials \mathbf{m}_1 , \mathbf{m}_2 and \mathbf{m}_3 , produced at each of the five electrodes by the three unit sources are marked with asterisk, the line of zero potential being the unit radius circle. The source waveforms from Fig. 3.1b are sampled at the rate of 256/s.

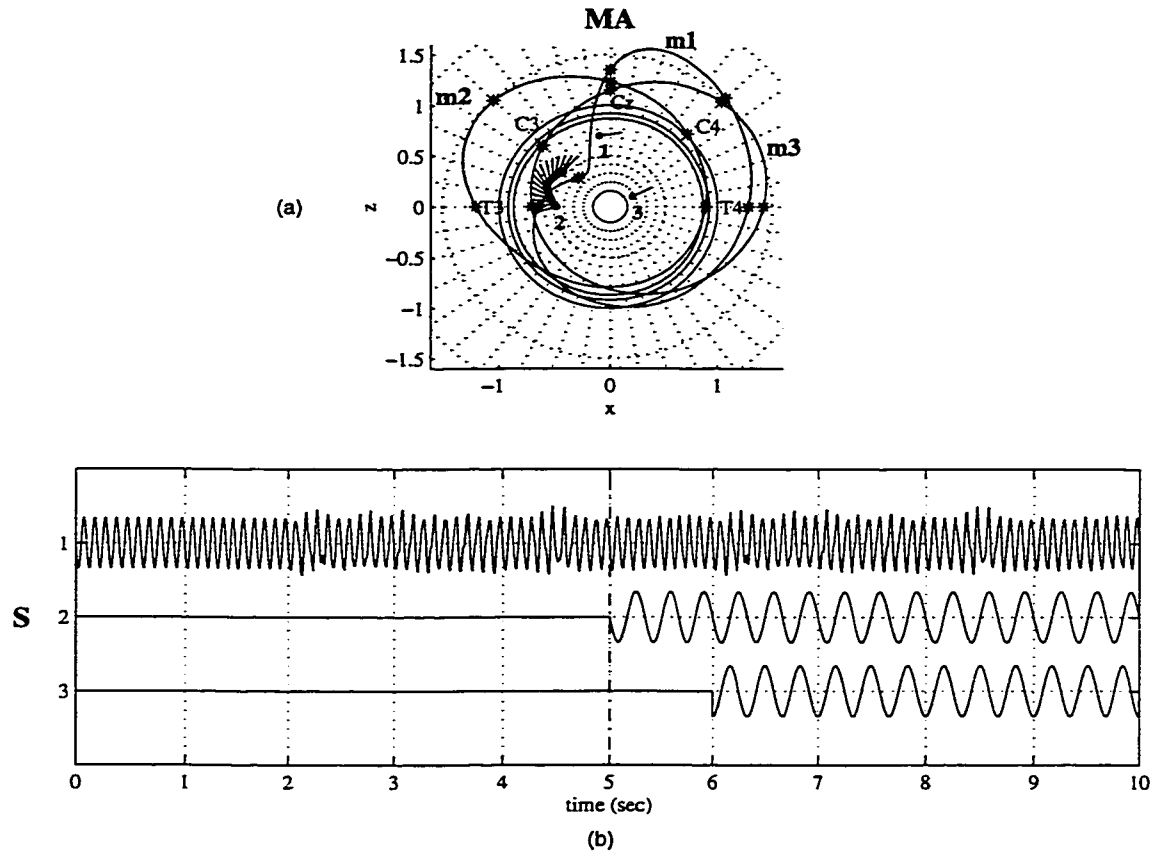


Figure 3.1. The potential images produced by three sources (a) and the corresponding source currents (b).

Figure 3.1 shows the locations, orientations and the moments of the three sources. The dipole source 1, \mathbf{m}_1 , is located at $x_1 = -0.1$ and $z_1 = 0.7$, is tangential (the angle between the radial line between the center of the slice and the orientation of the dipole is 90°) and is active for ten seconds. The first source waveform is a 10 Hz sinusoid in the first two seconds with superimposed frequencies from a real EEG waveform after this time, such that the frequency spectra of the three waveforms do not overlap. Source 1 is simulated as the normal source, responsible for the background activity. The magnitude of the background source was set so that it accounts for 53.41% of the variance in the last five seconds of the EEG, which is the highest variance contributed by the three waveforms.

The second source is a dipole-sheet current source. This source was simulated as the sum of correlated dipole sources of different orientations as shown in Fig. 3.1.a. The source waveform number 2 starts at five seconds and is a 3 Hz sinusoid. This source is considered abnormal and it accounts for 24.2% of the variance in the last five seconds of the EEG.

Source number 3, \mathbf{m}_3 , is a deep dipole source, located at $x_3=0.2$, $z_3=0.1$, radially oriented, also abnormal, starting at 6 seconds. The orientation and location of this source is chosen such that the potential at as many as possible electrodes is close to the potential of source \mathbf{m}_1 also for illustrative purposes, which are explained later. This third source waveform is of the same frequency as the second waveform but shifted in phase by 90° . The third source accounts for the least variance in the last five seconds of activity, 22.38%. It results that the sources account individually for 53.41%, 24.20% and 22.38% of the total variance in the last five seconds of activity.

The EEG in Fig. 3.2 is obtained by multiplying \mathbf{M} , \mathbf{A} , and \mathbf{S} shown in figure 3.1 as in equation 2.3 In this simulation the noise term is $\mathbf{E}=0$. The potentials at the electrodes are simulated with respect to the reference electrode Cz'. The vertical dotted line at 5 sec. delimits the normal, \mathbf{V}_n , and the abnormal, \mathbf{V}_a , EEG epochs.

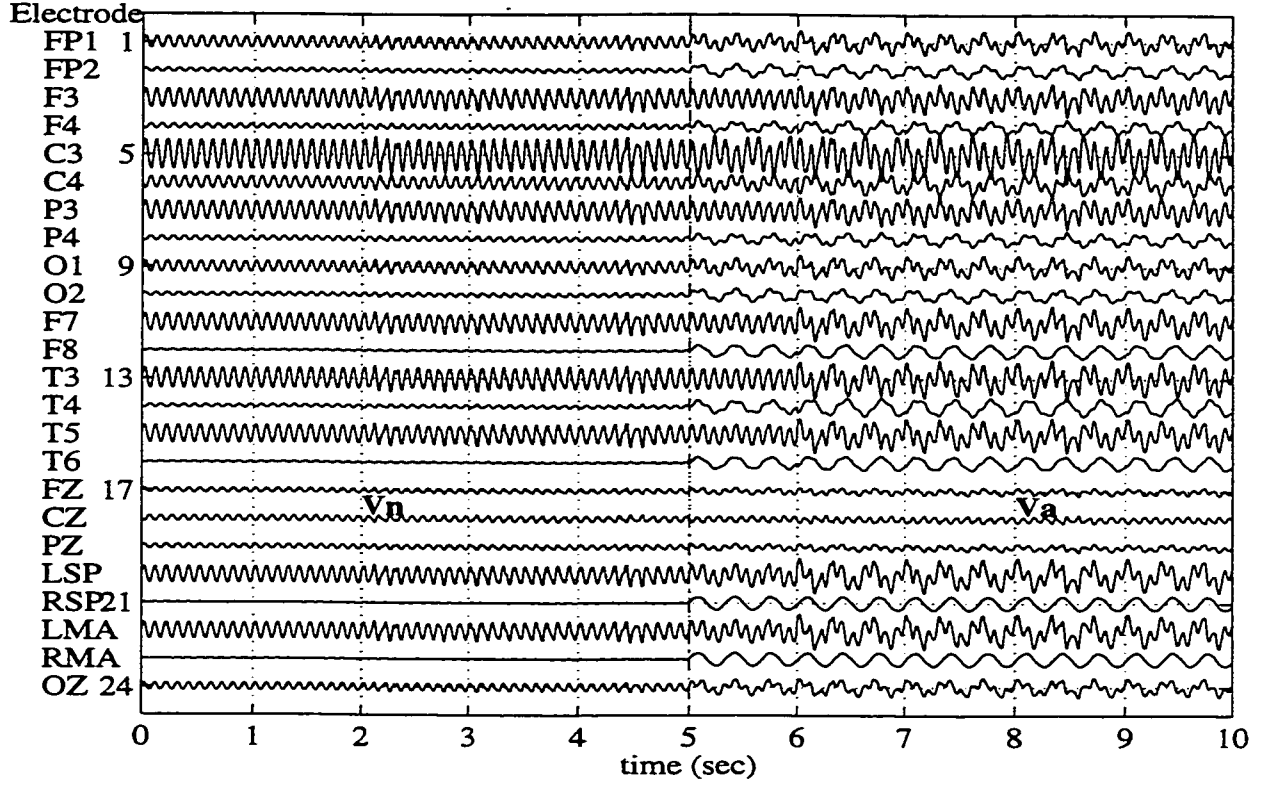


Figure 3.2. The EEG (V) simulated using the spatial and temporal components plotted in Figure 3.1.

3.1.2 The Principal Component Decomposition of the EEG

The abnormal epoch of the simulated EEG in Fig. 3.2, V_a , is decomposed as in equation 2.14 and the spatial and temporal patterns plotted in Fig. 3.3a and 3.3b respectively. The orthonormal basis vectors \mathbf{B} are determined by eigenvalue-eigenvector decomposition of the covariance matrix of V_a . Since three sources are active in the abnormal segment V_a , the rank of the covariance matrix is three. The rest of the $N-3$ eigenvalues are zero. The eigenvectors \mathbf{b}_1 , \mathbf{b}_2 , and \mathbf{b}_3 account individually for 56.9%, 31.5% and 11.6% of the total variance in V_a . These numbers differ from the variances accounted for by the three sources \mathbf{m}_1 , \mathbf{m}_2 and \mathbf{m}_3 . Applying the linear transformation 2.13, where $\mathbf{B}=[\mathbf{b}_1 \ \mathbf{b}_2 \ \mathbf{b}_3]$, to the EEG results in the three

orthogonal waveforms \mathbf{Y} shown in Fig. 3.3b. The eigenvalues are shown in the right side of the figure.

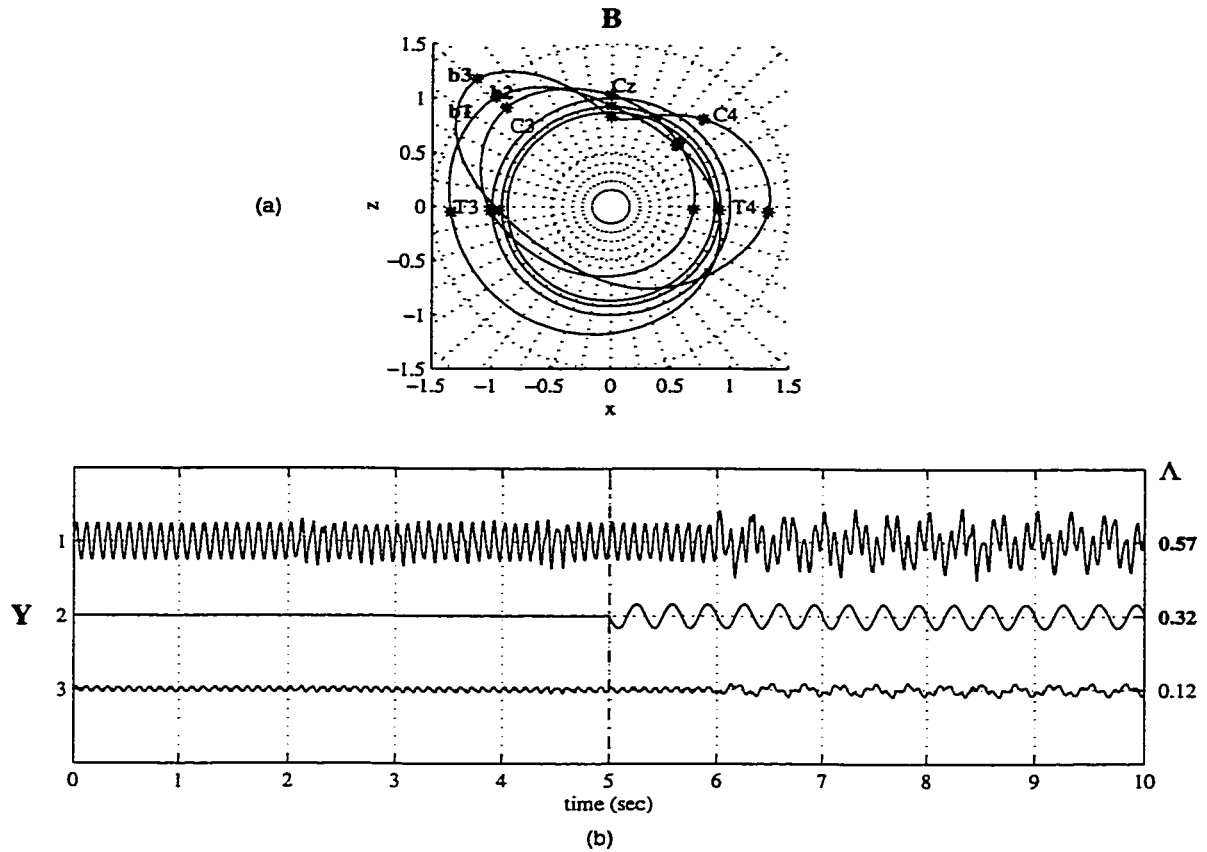


Figure 3.3. The Principal Component spatio-temporal decomposition. (a) The spatial patterns. (b) The temporal patterns

As shown in section 2.1.2, the first principal component points along the direction of maximum variance in the EEG. Since the normal source \mathbf{m}_1 accounts for the maximum variance in \mathbf{V}_s , it is expected that the waveform corresponding to the first eigenvector \mathbf{b}_1 will contain predominantly the temporal pattern \mathbf{s}_1 . By visually inspecting the first waveform it can be observed that the third source waveform, \mathbf{s}_3 , is also strongly present in the first PC waveform. One thing to consider in order to explain this effect is that the voltage at the electrodes is the only information available in the analysis. As mentioned before, the source

images \mathbf{m}_1 and \mathbf{m}_3 were simulated such that their potential values would be close at as many electrode sites as possible, at the same time having different potential profiles at points between the electrodes. This also determines the appearance of the first PC waveform. The second PC waveform looks similar to the source waveform s_2 .

The spatial components \mathbf{B} are interpolated and their profiles in the slice $y=0$ plotted in Figure 3.3.a. It is expected that the spatial component profiles \mathbf{B} and the temporal components \mathbf{Y} would relate to the aspect of the source images \mathbf{M} and waveforms \mathbf{S} . Indeed, if the first principal component b_1 , corresponding to the first PC waveform from \mathbf{Y} , is inverted and the values are compared to the values of the source images (Fig. 3.1) at the five visible electrodes, b_1 approaches \mathbf{m}_1 and \mathbf{m}_3 at all of the electrodes except C3. The spatial component b_2 has the same profile as \mathbf{m}_2 , with scaled down values, which is reflected in the second PC waveform and slightly smaller variance accounted for.

The aim is to separate the PCs that span the signal and noise subspaces, based on the variances accounted for in the abnormal EEG epoch. In order to do this, the cumulative sums of the variances accounted for by the eigenvectors are calculated: 57%, 89% and 100%. The first two eigenvectors are selected as signal vectors, the last eigenvector being considered as noise vector, based on the small variance accounted for in \mathbf{V}_a .

The PC decomposition of the EEG responsible for the abnormal activity can be then written as in equation 2.15 - 2.16, where

$$\begin{aligned}
\mathbf{B}_s &= [\mathbf{b}_1 \quad \mathbf{b}_2] \\
\mathbf{Y}_s &= \begin{bmatrix} y_1 \\ y_2 \end{bmatrix} \\
\Lambda_s &= \begin{bmatrix} 0.57 & 0 \\ 0 & 0.32 \end{bmatrix}
\end{aligned} \tag{3.1}$$

where the noise terms are ignored. The question to be posed now is whether this delimitation of the signal space is suitable for isolating the sources that are abnormal, that is the sources that become active at 5 respectively 6 seconds. It is clear that since the normal source accounts for maximum variance in the EEG, as it mostly happens in practice, using this decomposition the first principal component does not isolate an abnormal source. In Chapter 3.2 the application of the PC decomposition in source localization is performed and is discussed.

3.1.3 *The Common Spatial Pattern Decomposition*

It is expected that the PC decomposition will not isolate the abnormal spatio-temporal components. On the contrary, the most significant spatial component, the first PC, clearly corresponds to background activity, which is considered to be noise. In the attempt to eliminate the background activity and isolate the abnormal signal sources the CSP decomposition, described in Chapter 2.1.3, is applied to the simulated EEG, Figure 3.2 The result is shown in Figure 3.4.

Comparing both the profiles of the spatial patterns and the temporal waveforms in Fig. 3.4 with the source images in Figure 3.1, the similarity is evident. The first CSP, c_1 , has similar profile with \mathbf{m}_2 , and the corresponding waveform $Z1$ is almost identical to s_1 . c_1 points in the direction of maximum variance (100%) in the abnormal EEG \mathbf{V}_a and minimum variance (0%) in the normal EEG, \mathbf{V}_n .

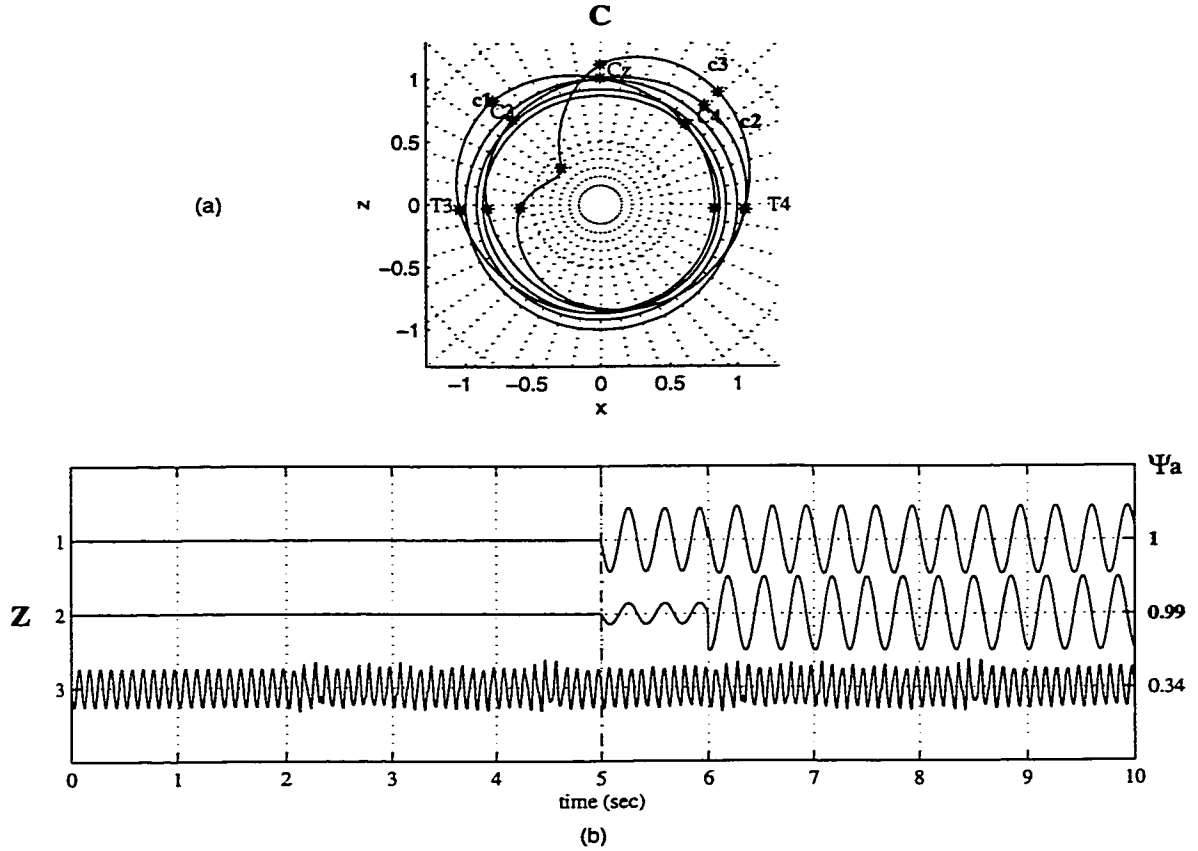


Figure 3.4. The Common Spatial Pattern Decomposition. (a) The Common Spatial Patterns; (b) The Temporal Patterns

The second CSP component, c_2 , which has similar profile to m_3 , accounts for the next greatest difference between variances in V_a and V_n . There is some difference in the appearance of the deep dipole source waveform s_3 and the second CSP waveform z_2 , which explains the percent variance of 99%, instead of 100% as expected, if the CSP decomposition perfectly retrieved m_3 and s_3 .

The third CSP, c_3 , accounts only for 34% variance in the abnormal EEG and 66% variance in the normal EEG. The profile of this vector resembles remarkably well the image profile of the normal source m_1 . Since this vector c_3 accounts for more variance in the normal EEG than in the abnormal EEG, it is selected as spanning the noise space and is part of C_e .

according to equations 2.27 - 2.28. The CSP decomposition and the covariance matrix of the EEG responsible for abnormal activity can be then written in terms of the signal vectors \mathbf{C}_s , \mathbf{Z}_{as} , and Ψ_{as} respectively. The eigenvalues that correspond to the signal spatial components are written in bold characters in Figure 3.4. The spatial components that span the signal space, the corresponding temporal components and the eigenvalues are:

$$\begin{aligned}\mathbf{C}_s &= [\mathbf{c1} \quad \mathbf{c2}] \\ \mathbf{Z}_{as} &= \begin{bmatrix} \mathbf{Z1} \\ \mathbf{Z2} \end{bmatrix} \\ \Psi_{as} &= \begin{bmatrix} 1 & 0 \\ 0 & 0.99 \end{bmatrix}\end{aligned}\tag{3.2}$$

With respect to the EEG model, it can also be observed that the source that accounts for maximum combined variance in the abnormal EEG and minimum variance in the normal EEG is \mathbf{m}_2 (24.2%-0%=24.2%). As opposed to \mathbf{m}_2 and \mathbf{m}_3 , the normal source \mathbf{m}_1 , present both in the normal and abnormal EEG, accounts for more variance in the normal EEG (100%) than in the abnormal EEG (53.41%). This indicates that the CSP $\mathbf{c3}$ that points in the direction of \mathbf{m}_1 spans the noise space. This verification of the fact that the CSPs point in the direction of the maximum variance accounted for by the current sources in the abnormal EEG and minimum variance in the normal EEG is important as it gives more confidence in analyzing real data. This is the case when sources that become active at one point in time are to be isolated, as in epilepsy.

3.2 Source Localization - Simulation Results

In this subchapter the three methods of source localization described in Chapter 2.2 are illustrated using the EEG decompositions of the simulated EEG. The objective is to

accurately localize the two abnormal sources \mathbf{m}_2 and \mathbf{m}_3 . For all of the simulated source localizations the inner shell of head model is sampled at 0.5 cm. In the case of LORETA, only the upper half of the head model is sampled, at 1cm. Therefore the two dipole sources \mathbf{m}_1 and \mathbf{m}_3 are located on the spatial grid, and the SLI is expected to be maximum at these locations if the sources are localized accurately. Another consideration is the GOF. It was assumed in Chapter 2 that the *SLI* should exceed the value of 2 in order to obtain a good fit. This measure of GOF for the case of noiseless simulations and where the same model is used for both simulating the EEG data and for source localization might not appropriate. For the case of noiseless simulated data the maximum admissible error is set at 0.001, which corresponds to a $GOF \geq 0.999$ and a *SLI* equal to at least 3. Any peak higher than this value is considered a source location, which can easily be verified knowing where the sources are located.

3.2.1 Single Dipole Fitting

In order to illustrate the Single Dipole Method described in 2.2.1, the PC decomposition of the EEG from section 3.1.2 is used. First all of the eigenvectors are used in the source localization procedure. That is, the source location index is calculated as

$$SLI(x, y, z) = -\lg \frac{\bar{J}_1(x, y, z)}{\|\hat{\mathbf{M}}\hat{\mathbf{M}}^*\mathbf{B}\mathbf{A}\|_F^2} \quad 3.3$$

where \bar{J}_1 is the squared Frobenius norm of the projection of all three eigenvectors on the left null space of the candidate source at each grid location, as in equation 2.34. Since the waveform matrix \mathbf{Y} is orthogonal, this projection is the same as projecting the whole abnormal EEG \mathbf{V}_a on the left null space of the candidate source. The mesh of the SLI on the vertical slice $y=0$, containing the minimum of \bar{J}_1 is shown in Figure 3.5a.

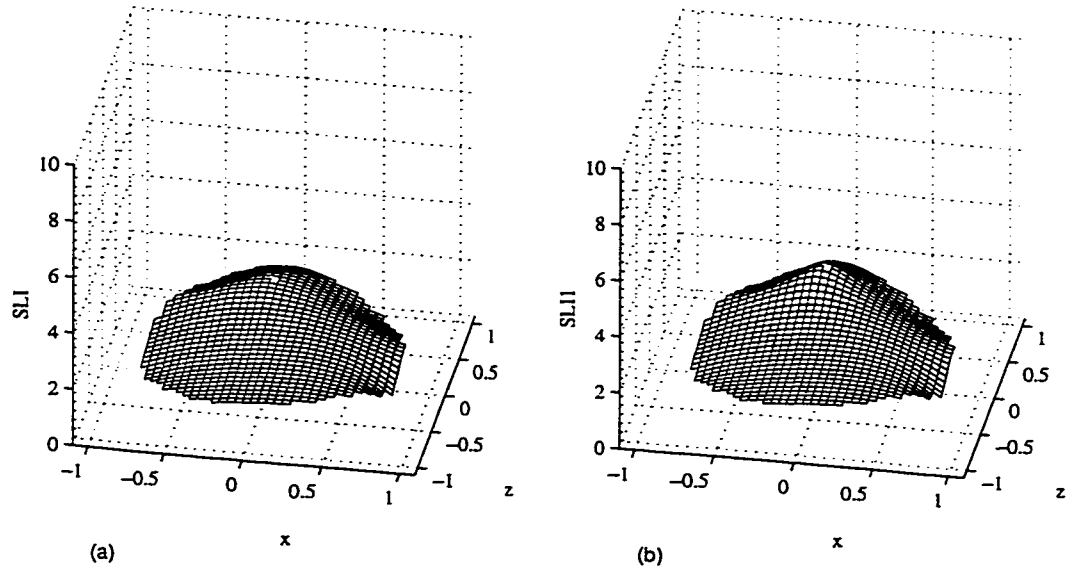


Figure 3.5. The topography of the *SLI* using Single Dipole Fitting for the three sources of the simulated EEG. (a) All three eigenvectors corresponding to nonzero eigenvalues are used. (b) Only the first two eigenvectors are used.

As the EEG is produced by three sources, the Single Dipole Fitting localizes an equivalent dipole. This equivalent dipole is located at $x=-0.1$, $y=0$, $z=0.5$, that is 2 cm distant on the Z axis from the normal dipole source \mathbf{m}_1 . This result is not surprising, as the first principal component that accounts for 57% of the total variance in \mathbf{V}_a and points in the direction of maximum variance, that is towards source \mathbf{m}_1 , and the fact that the other two sources \mathbf{m}_2 and \mathbf{m}_3 are located approximately symmetrically and towards the origin with respect to the Z axis. The *SLI* is in this case 2.3, which is another indication that the localized dipole is not at a true source location. Figure 3.5b shows the localization using only the signal PCs and the corresponding eigenvalues, from equations 3.1 substituted in equations 2.35 and 2.36. The

localization result is the same, with the difference that the source location index increased to 2.8.

3.2.2 *Multiple Dipole Fitting*

As explained in section 2.2.2, the sources of EEG can be individually localized if a unit dipole model is projected at each grid point on the left null space of the spatial components selected as spanning the signal space. Here the MUSIC algorithm is applied with both the PC and CSP decomposition of the EEG.

First the noise projector matrix is formed using all three PCs of the abnormal EEG and the topography of the SLI is shown in Figure 3.6a. For this case the function minimized is similar to equation 2.42:

$$\tilde{J}_2 = \left\| (\mathbf{I} - \mathbf{B}\mathbf{B}^+) \hat{\mathbf{M}}\mathbf{a} \right\|_F^2 \quad 3.4$$

In this equation it is possible to use the transpose instead of pseudoinverse since for an orthonormal matrix the pseudoinverse is equal to the transpose of the matrix. At each grid location the optimum orientation of the dipole, that minimizes \tilde{J}_2 , is found. The SLI in this case is similar to equation 2.50

$$SLI(x, y, z) = -\lg \frac{\tilde{J}_{2\min}(x, y, z)}{\left\| \hat{\mathbf{m}}_a \right\|_2^2} \quad 3.5$$

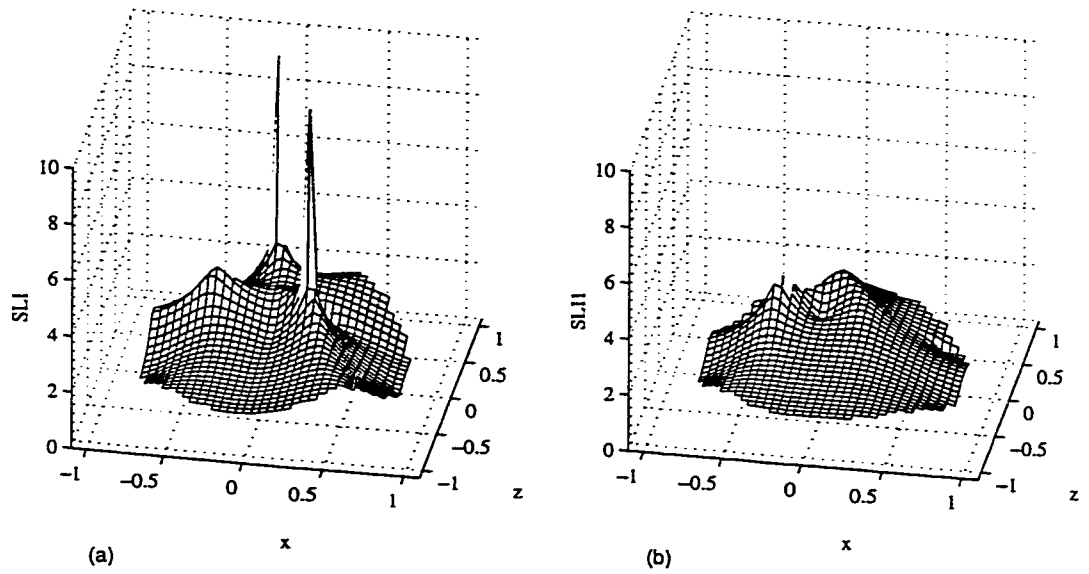


Figure 3.6. The topography of the *SLI* using Multiple Dipole Fitting for the three sources of the simulated EEG. (a) All three eigenvectors corresponding to nonzero eigenvalues are used. (b) Only the first two eigenvectors are used.

All three EEG sources are localized. The two dipole sources are accurately localized and a minimum of zero is obtained at the locations of \mathbf{m}_1 and a minimum very close to zero at the location of the deep dipole source \mathbf{m}_3 . The orientations are the same as for the simulated dipole sources. The *SLI* for the deep radial dipole source is only 2% smaller than the *SLI* for the more superficial, tangential, dipole source. The distributed dipole source is localized at $x=-0.4$, $y=0$, $z=0.25$, oriented at 162° , with a *SLI*=3.33.

In Figure 3.6.b the topography of the *SLI* in the slice $y=0$, when only the eigenvectors \mathbf{B}_s are used in the projection matrix, is shown. The locations, orientations and *SLI* of the two sources are $x_1=-0.35$, $y_1=0$, $z_1=0.25$, oriented at 167° , *SLI*₁=3.13 and $x_2=-0.05$, $y_2=0$,

$z_2=0.55$, oriented at 82° , $SLI_1=2.66$. The distributed source is located at 0.5 cm from the previous case and the value of the SLI indicates that this can be considered a source location. The second source is misslocalized both on the X and Z directions.

This example shows that PC may not localize the signal vectors responsible for the abnormal activity unless all of the eigenvectors that span the whole signal space, that is all of the eigenvectors that correspond to eigenvalues different from zero are used in the projection matrix. This is because of the allocation of the first PC to the abnormal signal space. This would not be acceptable in the case of real data, unless the data could be previously filtered such that no background or artifactual activity would be present in the abnormal epoch or these components account for small variances in the abnormal EEG.

In contrast to using the PC with MUSIC, when the CSPs C_s are used in the projection matrix in equation 2.42 both abnormal sources are correctly localized. The SLI_s , calculated for each grid point using equation 2.50, resulted in a maximum at the location of the dipole and 3.13 at the location of the equivalent dipole for the distributed source. The calculated dipole orientation is radial. For the equivalent dipole of the dipole sheet the orientation is found 167° . The topography of the SLI for this case is shown in Figure 3.7a.

3.2.3 *LORETA*

In the previous section it was shown that both the abnormal dipole source and dipole sheet can be localized if the CSPs are used in the projection matrix. However, the concern is the relatively low peak obtained for the distributed source. Since LORETA is a minimum norm based method, there is no requirement for the sources to be dipoles or to be uncorrelated. Therefore it is expected that the dipole sheet will be better localized using this method.

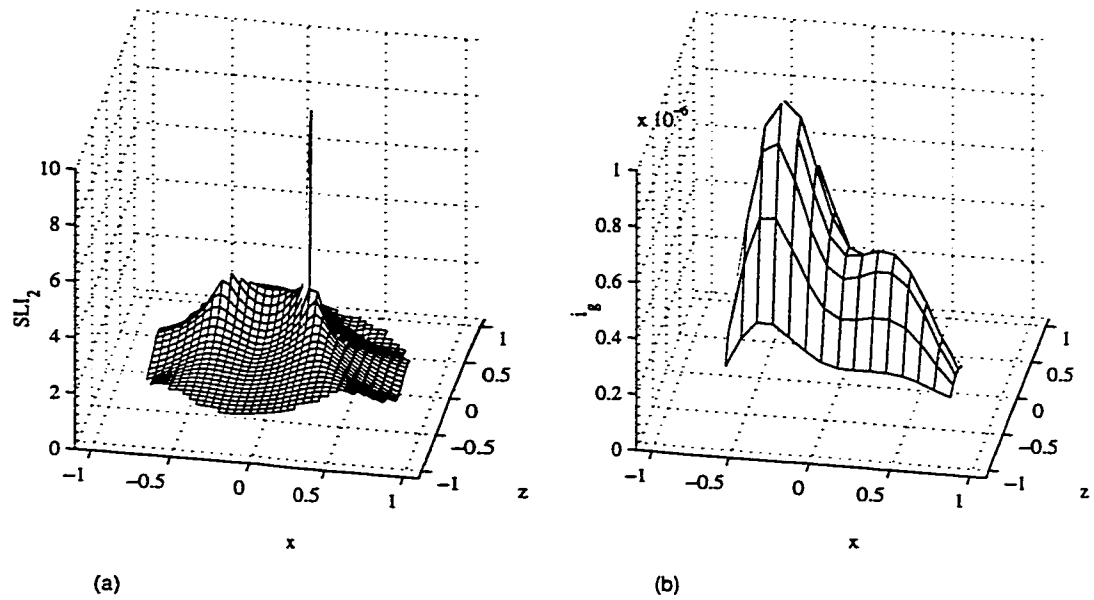


Figure 3.7. (a) The topography of the SLI using MUSIC with CSP. (b) The Topography of the LORETA solution using CSP.

The variance of the source current density is calculated as in equation 2.64 and for each grid point as in 2.65. The topography of the LORETA solution is shown in Figure 3.7.b. It can be observed that the dipole sheet is better localized with LORETA, whereas for the dipole source LORETA gives a blurred solution, the dipole source being better localized with MUSIC.

3.2.4 Seizure Spread

In the case of seizure data, the electrical activity characteristic to the seizure may spread from one part of the brain to another. The EEG simulated is an example of such a scenario. First the background source is active, and then the dipole-sheet located in the left side and the deep dipole source become active afterwards. In order to determine the dynamics of the

abnormal activity, the CSP and the waveform corresponding to the background pattern are spatially filtered out from the simulated EEG. Each second of abnormal filtered EEG is then decomposed using PC and all the resulting PCs used with the MUSIC algorithm. For the segment of EEG between 5-6 seconds only one PC was found and the topography of the SLI is shown in Fig. 3.8a. For the EEG segment between 6-7 seconds two PC were found and used for localization. However, due to the big difference between the peak obtained for the deep dipole source and the dipole sheet, the location of the dipole sheet peak cannot be seen in Fig. 3.8b using this type of map, which was chosen to illustrate the determined source orientations and the spread of the abnormal activity.

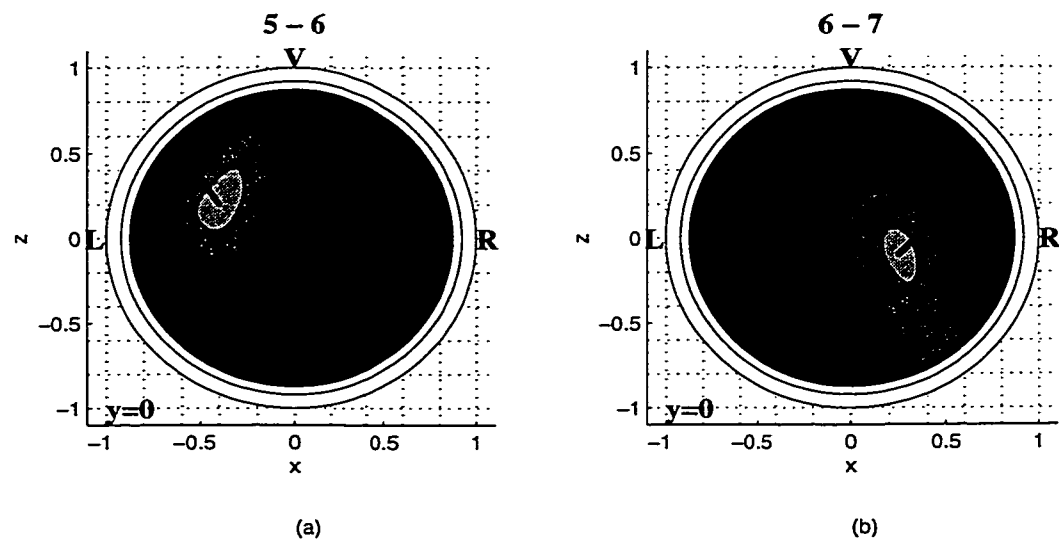


Figure 3.8. The dynamics of the abnormal electrical activity in the last five seconds of the EEG

4 REAL DATA RESULTS

4.1 Introduction

The adult patient for whom the source localization was performed and is presented in this chapter was discussed in the weekly Seizure Conference, which is part of the Comprehensive Epilepsy Program, held at the University of Alberta Hospital. All of the patients analyzed in the Conference are surgical candidates, in which the drug therapy has failed to control the seizures, the quality of life for these patients being severely affected by the frequency and the extent of the seizures.

The clinical routine involves the expertise of epileptologists, radiologists, psychologists and neurosurgeons. The ultimate goal of the clinical evaluation of an epileptic patient is to determine if and when the patient should undergo surgical therapy, the area in the brain where the seizure originates from, and the extent of the resection (neuro-surgical procedure) to be made. In some of the cases, especially in the case of pediatric patients, the decision is not the easiest. Considerations such as lack of knowledge about the location of speech and memory make the neurosurgeons treat these cases with increased precaution as the resection might be of a potential risk for the patient. In some cases further trials of drug therapy are considered.

However, in many of the patients an estimate of the location in the brain where the seizure originates can be obtained. The major disadvantage of the procedure used is that it is highly invasive due to the fact that it can involve intracranial recording or/and angiography. The intracranial recording is an invasive technique of acquiring the EEG, using needle electrodes. Angiography is a technique that involves the injection of a substance in the patient's body in order to better visualize the blood vessels, which can be damaged in some epileptic patients.

In the following sub-chapters the clinical procedure, the results using the proposed noninvasive source localization methods and the validation of the results obtained will be presented.

4.2 Clinical procedure

As mentioned in the above introduction, the clinical procedure in source localization involves extended information about the electrical activity of the patient's brain, the brain structure and the development of its neuro-psychological functions. The medical history of the patient is also considered in the clinical evaluation.

The recording of the EEG is performed in the so-called Telemetric Unit. The aim is to record the EEG before and during the seizure. The patient is permanently attached to an array of electrodes, in this case 25 electrodes. A computerized system detects the inter-ictal EEG spikes that appear prior to the occurrence of a seizure and the EEG recording commences. The telemetric system also includes the video monitoring of the patient in order to observe the clinical manifestations of the patient during the seizure, which can bring very important insight in the determination of the location of the epileptic activity, based on the a-priori knowledge of the sensory-motor areas in the human brain. The EEG and video recordings are synchronously acquired. The system permits the concomitant visualization on the split view of a monitor screen of both the EEG and the patient during the seizure so that the correlation between the EEG and the clinical manifestations of the disease can be observed.

The Magnetic Resonance Imaging and sometimes Computer Tomography, Positron Emission Tomography or Single Photon Emission Computed Tomography scans of the head are used to determine whether abnormalities can be observed. The neuro-psychological

assessment is then presented. The information provided as the result of verbal and performance IQ tests along with the neuro-motor tests can lead to important conclusions about the development of various areas of the patient's brain.

4.3 The seizure onset and source localization procedure

The procedure requires temporal and spatial localization. The temporal localization refers to the localization in time of the seizure onset, within the recorded EEG. The source localization requires the delimitation of the signal space by finding a set of spatial components prior to applying the source localization methods.

The first step in this procedure presupposes the band-pass filtering of the measured EEG in order to reduce the number of sources responsible for the background EEG and eliminate artifactual components. In the second step of the procedure, an epoch of the filtered EEG, that most probably contains the seizure onset, is retained and decomposed into spatial and temporal components. The spatio-temporal decomposition is based on spatial patterns common to both the pre-ictal (normal - preceding the seizure onset) and ictal (abnormal - following the onset of the seizure) EEGs. The spatial components that account for more variance in the ictal EEG than they do in the pre-ictal EEG are retained and used to localize the seizure focus.

4.4 Real data analysis

The method has been applied on EEGs recorded from eight patients with focal epilepsy and a total of eighteen seizures. Only one patient is analyzed here using one seizure EEG recording. The digital EEGs were acquired at 200 samples/sec using the 25-electrode montage shown in Chapter 1. The raw EEG was recorded for approximately one minute and only 10 seconds were selected and shown in this work. The selection of the 10-second raw

EEG epoch, shown in Figure 4.1, was made such that the epoch would contain the subsequently determined seizure onset.

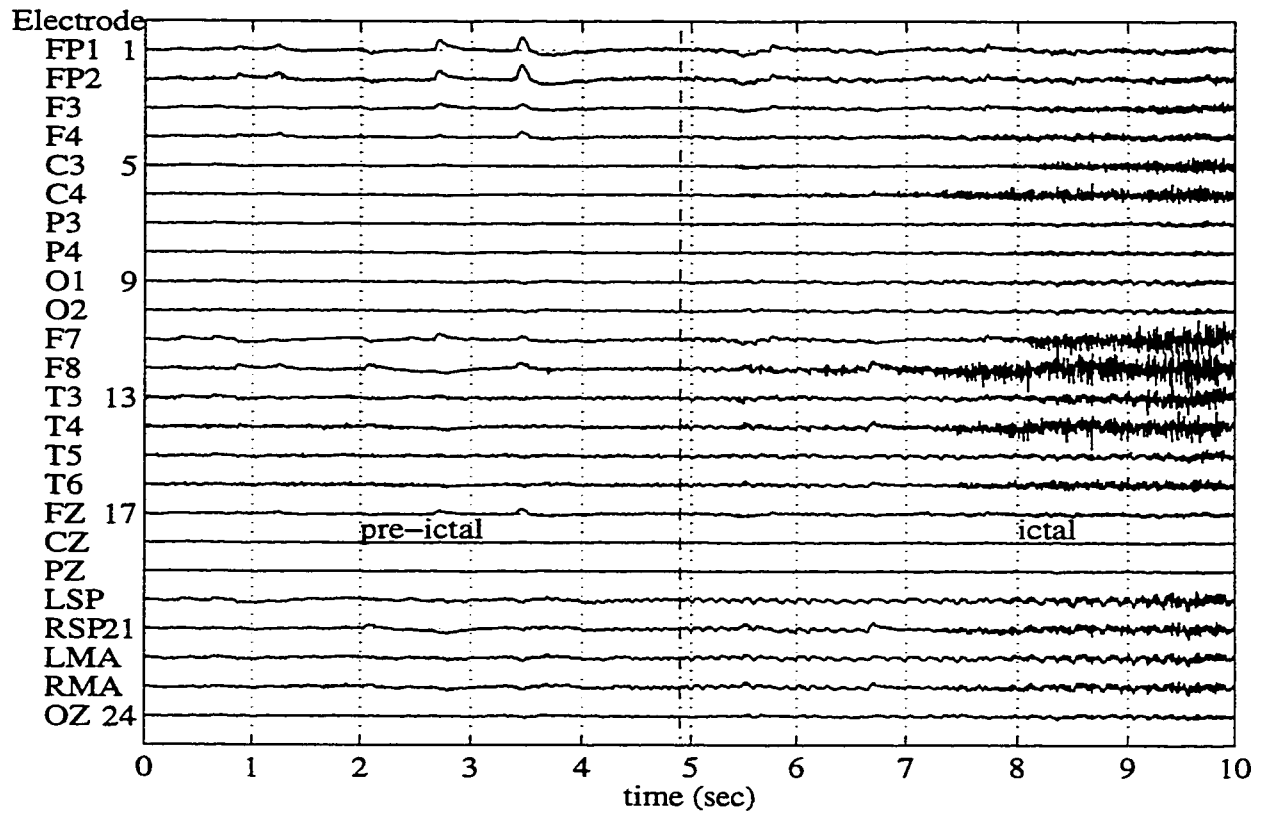


Figure 4.1. The epoch from the recorded EEG containing the seizure onset

The seizure onset, which is thought to originate in the epileptic focus is marked in the figure by a vertical dotted line. The normal (pre-ictal) and the abnormal (ictal) segments of the EEG are also marked in the figure. The electrodes at which the data was acquired are listed on the left side of the figure. As it can be seen, no conclusion can be drawn about the seizure onset from the raw data.

4.4.1 Seizure onset localization

Although the highest voltages can be observed as occurring the earliest at the right-frontal, right-temporal and right-central electrodes, this is not necessarily an indication that the seizure

would lateralize in the right side of the brain. The high frequency and amplitude recorded activity possibly could result from muscle artifact and the patient's motor manifestation during the seizure. Yet, the seizure onset may be contained by this epoch and if we were to be limited only to the information from this seizure one interpretation would be that the seizure would be localized to the right antero-temporal region with some spread to the left or, another interpretation would be that the seizure is bilateral, first starting on the right and then on the left side of the brain. Neither the mastoidal nor the sphenoidal electrode recordings are more relevant for the onset and source localization.

4.4.1.1 *Band Pass Filtering*

The raw data was first filtered using a band pass filter between four and ten Hertz, which, in the case of this patient, was found satisfactory for the accurate source localization. The power spectrum of the filter is plotted in Figure 4.2.

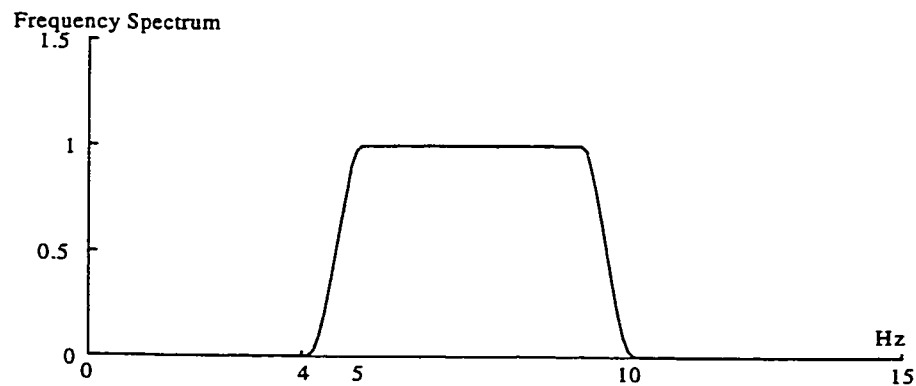


Figure 4.2. The power spectrum of the band pass filter used for the raw EEG filtering.

The frequency filtering used was performed in the attempt to eliminate the sources present that are not relevant to the seizure onset and yet preserving the waveform patterns characteristic to the ictal EEG. The 10-second frequency filtered EEG epoch that clearly contains the seizure onset is selected and is shown in Figure 4.3.

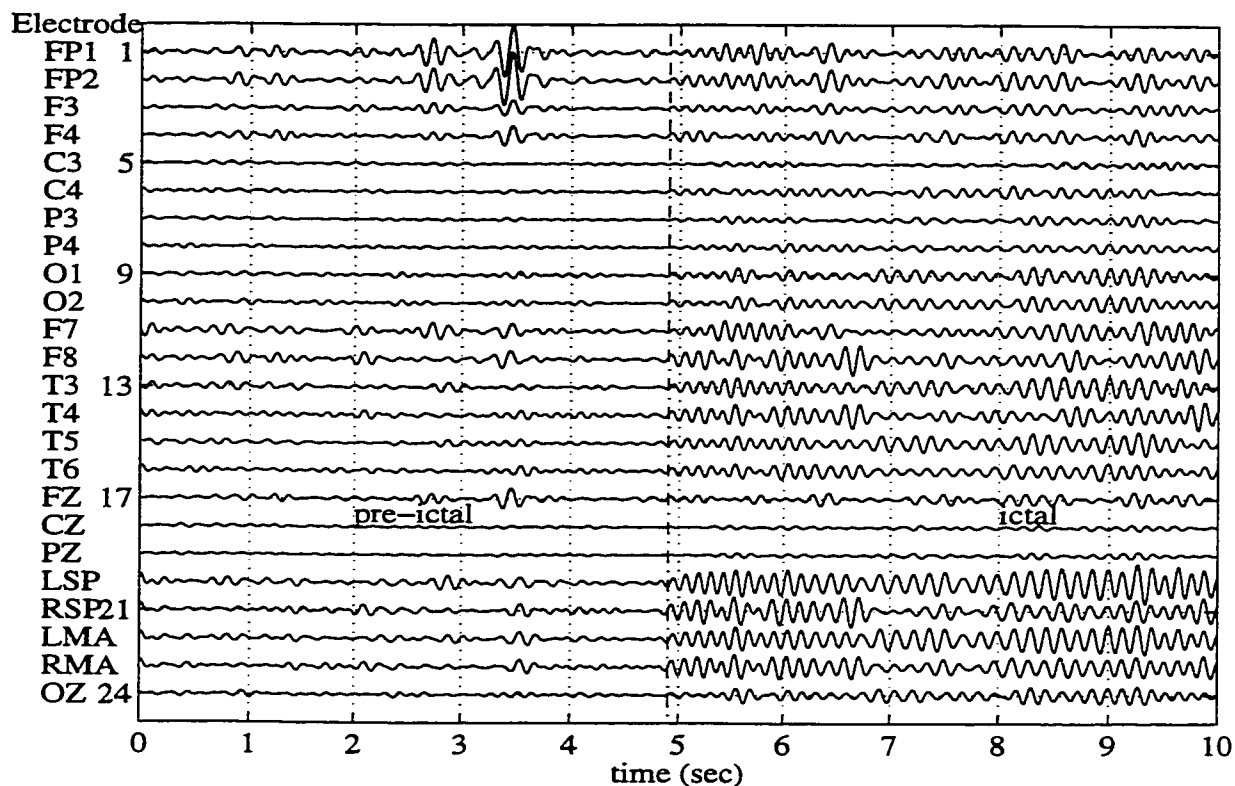


Figure 4.3. The frequency filtered EEG epoch.

The frequency and the amplitude content of the EEG responsible for the epileptic activity can now be identified. However, the precise identification of the seizure onset, within fractions of seconds, is not yet possible and the presence of the artifacts, especially the strong frontal involvement resulting from eye fluttering, would introduce errors in the localization process and need to be suppressed.

4.4.1.2 *Spatial Filtering*

The method of Common Spatial Pattern filtering described in Section 2.1.3 is applied to the temporally filtered data in order to more accurately detect the seizure onset and select the spatio-temporal components responsible for the epileptic activity, the signal space, while filtering the remained artifacts and background activity, the noise space. By decomposing the

covariance matrix \mathbf{R} as in equation 2.18 it was determined that the rank of Λ_c and \mathbf{R} is eight. This is reflected in the number of spatial and temporal components resulting from the CSP decomposition.

The CSP filter applied to the temporally filtered EEG epoch reveals the temporal components, \mathbf{Z} , and the CSPs, \mathbf{C} . The resulting temporal components are presented in Figure 4.4. The percentage variance that each CSP accounts for in the ictal segment of the EEG as compared to pre-ictal is listed on the right side of the figure.

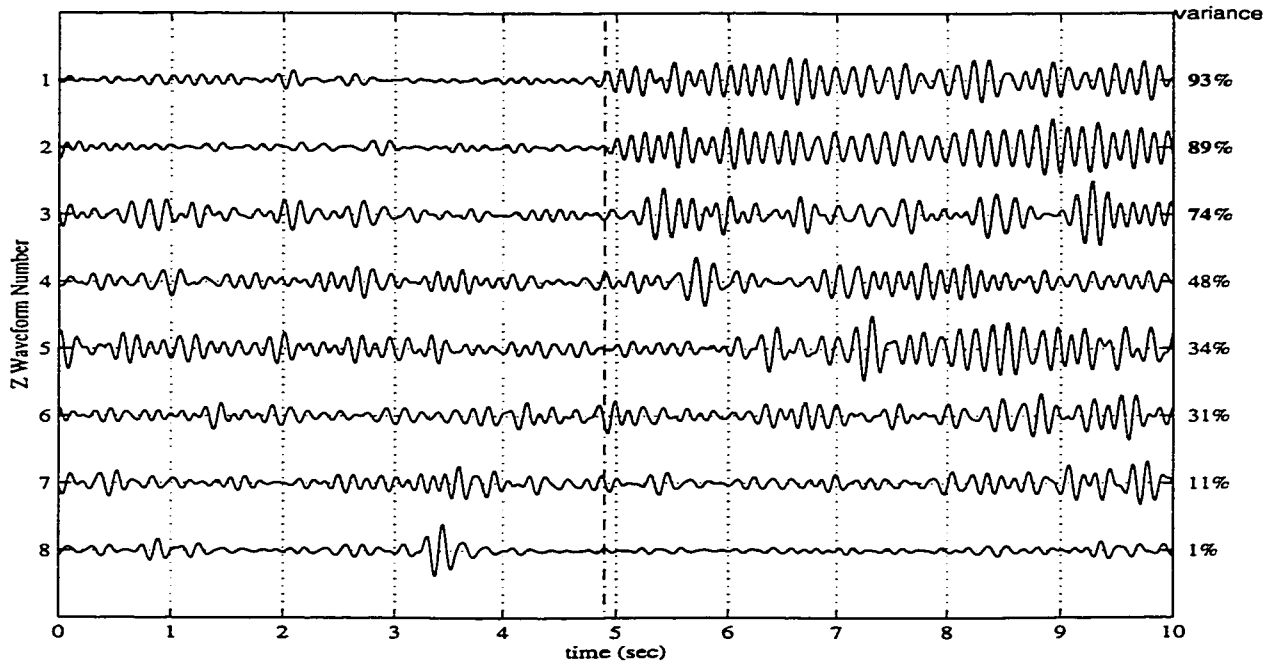


Figure 4.4. The EEG temporal components, \mathbf{Z} .

The first four corresponding spatial components are shown in Figure 4.5, where the axis notations N, R, L stand for Nasion, Right and Left respectively. The rest of the CSP components, that are not shown, point towards the frontal or left-frontal region, except the

spatial component that accounts for 31% in the abnormal epoch, which points toward the central-frontal region.

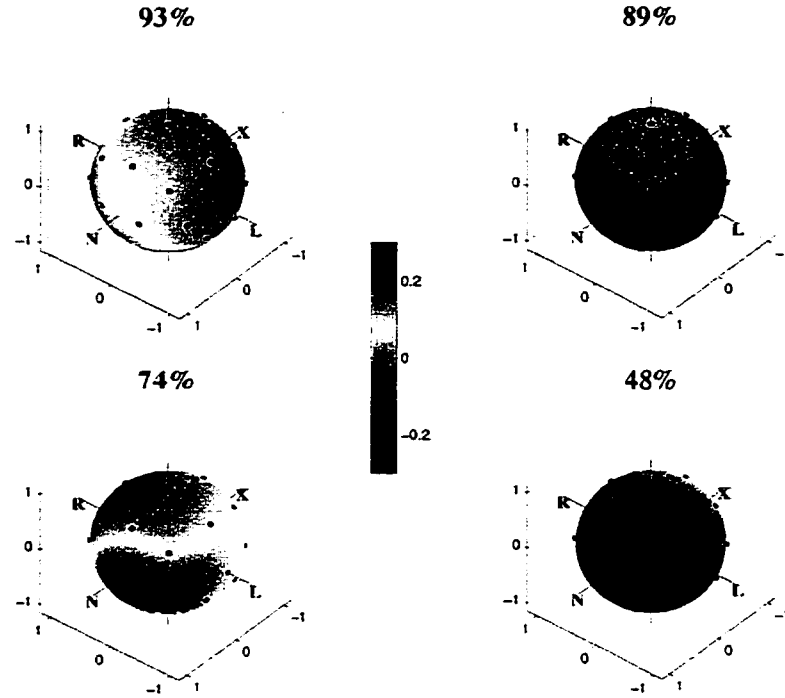


Figure 4.5. The first four spatial components of the frequency filtered EEG resulting from the CSP filtering.

The frequency filtered EEG (\mathbf{V}) is thus decomposed as:

$$\mathbf{V}_{24 \times 2000} = \mathbf{C}_{24 \times L} \mathbf{Z}_{L \times 2000} \quad 4.1$$

where L , in this case 8, is the number of current sources responsible for the frequency filtered EEG epoch of dimensions 24 electrodes \times 2000 samples. Only the common spatial patterns that account for more than 50% variance in the ictal and less in the pre-ictal, and their corresponding waveforms are retained as being significant for the epileptic activity and their variances are displayed in bold characters. The rest of the waveforms and their corresponding CSPs, which account for more variance in the pre-ictal than in ictal, the background and

artifactual components still present in the frequency filtered EEG, are filtered out. It can be observed that the eye artifact present in the fourth second is now filtered out, accounting for only 1% variance in the abnormal EEG epoch.

One great benefit of the Common Spatial Pattern filter is that it allows the evaluation of the time when the seizure starts, by visually inspecting the appearance of the waveforms. In the case of the presented patient the seizure onset can be determined visually around the 5th second in the frequency-filtered epoch. By successively assuming the seizure onset around this time, and performing CSP decomposition and source localization using the MUSIC algorithm, the found best fit was for the seizure onset localized at 4.9 sec.

It is thought that an EEG with a specific frequency and amplitude pattern consistent for three seconds indicates epileptic activity. When the ictal segment was considered three seconds from the seizure onset, and symmetrically for the pre-ictal segment, the CSP filtering result consisted of four waveforms that accounted for over 50% variance in the ictal EEG epoch (94%, 85%, 68%, 61%) where the last two waveforms clearly contained normal activity. The MUSIC algorithm using the four CSP resulted in a SLI of 2.18. However, the CSP filtering performed by delimiting the normal and the abnormal epoch also at 4.9 seconds but using only two seconds of abnormal activity resulted in the best fit for this seizure data. In this case the CSP filtering resulted in only three waveforms accounting for variance higher than 50% in the ictal epoch: 93%, 89% and 74% and smaller variance in the pre-ictal EEG epoch (Figure 4.4). The source localization using the MUSIC algorithm resulted in the highest SLI (2.29).

The frequency and spatially filtered EEG, reconstructed using only the first three spatial and temporal components, is presented in Figure 4.6 and is the result of the matrix multiplication in equation 4.1, where L is equal to 3.

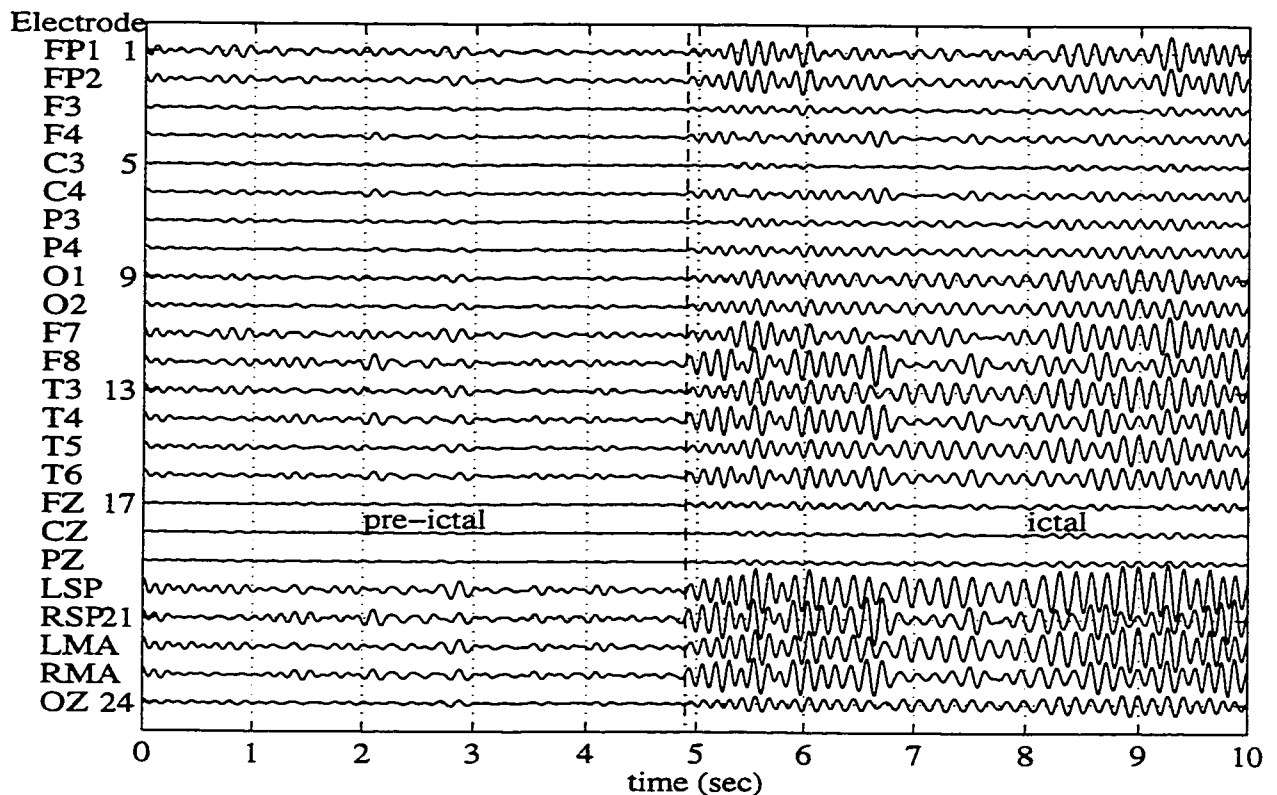


Figure 4.6. The reconstructed EEG from the first three spatio-temporal components.

By visually inspecting the reconstructed EEG one can observe the presence of consistently strong signal at the electrodes placed on the left side of the head: LSP, T3, LMA, T3, T5, F7. The interpolated images of the spatial components on a sphere (Figure 4.5) indicate strong activity on the left and right side, mostly right and left antero-temporal, with some left frontal involvement. However, there is still no indication about the location in the brain of the activity that produced these maps. This is where the source localization methods described in Chapter 2 are used.

4.4.2 Source localization

The source localization was performed using the three methods described in Chapter 2 and the results are to be compared.

4.4.2.1 Single Dipole Fitting

The first method applied is the Single Dipole Fitting. As described in Chapter 2.2.1, a linear combination, \mathbf{BA} , of the eigenvectors of the EEG is used for localizing the seizure focus. Here, this is performed by retaining the first principal component of the ictal segment of the reconstructed EEG shown in Figure 4.6. The principal spatial component \mathbf{b} (shown bilateral) and its corresponding waveform are presented in Figure 4.7.

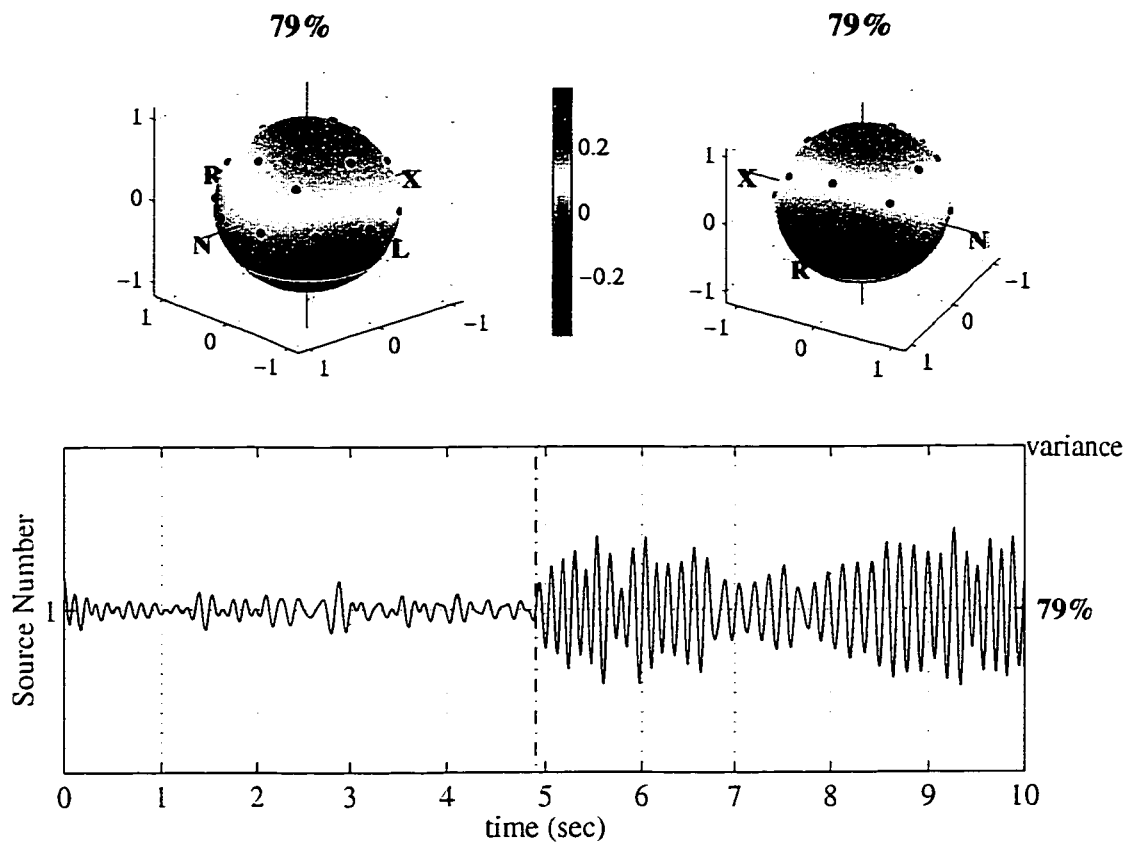


Figure 4.7. The First Principal Component \mathbf{b} and its corresponding waveform

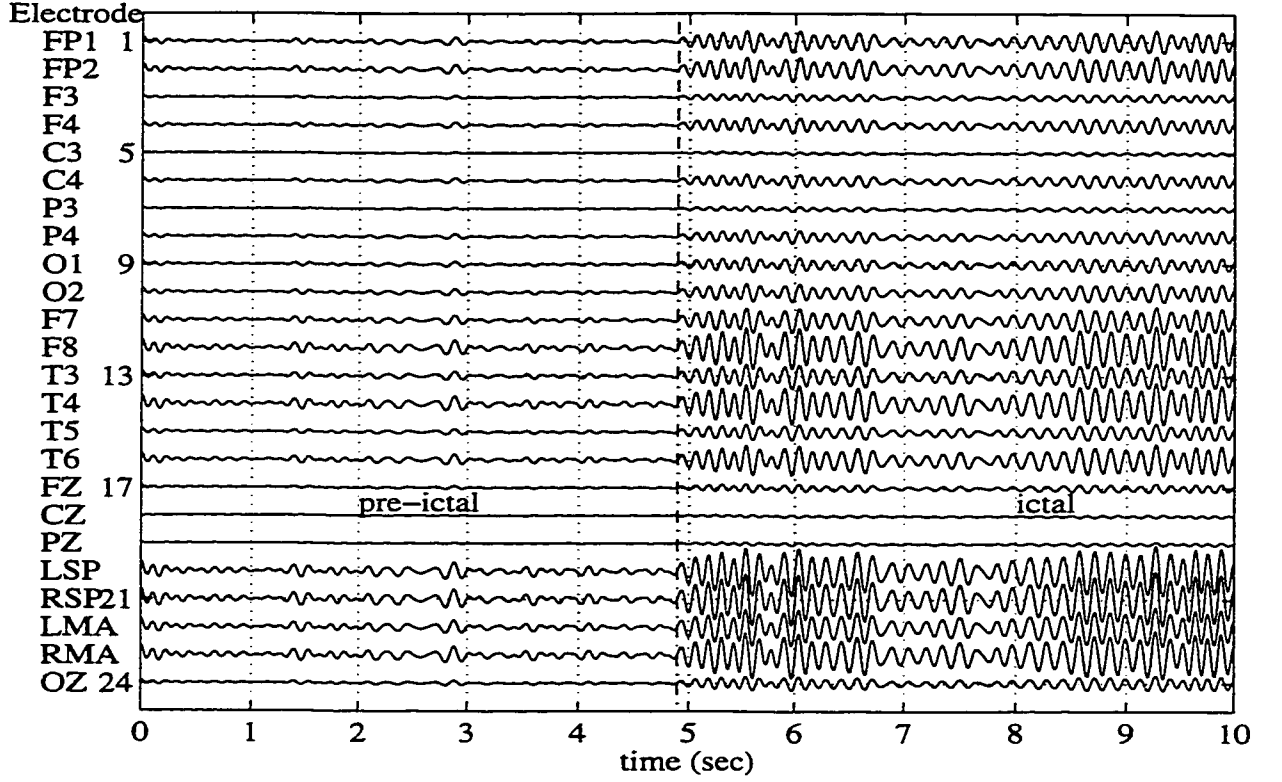


Figure 4.8. The reconstructed EEG from the first Principal Component \mathbf{b} and its corresponding waveform

The minimum obtained at the closest grid point location is given by the minimization function below, in which $\lambda_s=0.79$.

$$J_1 = \left\| (\mathbf{I} - \hat{\mathbf{M}}\hat{\mathbf{M}}^*) \mathbf{b}_s \lambda_s \right\|_F^2 \quad 4.2$$

The significance of each term and the minimization process was described in Chapter 2.2.1. The source location index formula applied to the calculated minima used to visualize the slices that contain the estimated source location is given in equation 2.36.

The image of the SLI_1 distribution on the horizontal and the vertical slice containing the maximum using the Single Dipole Fitting method is plotted in Figure 4.8. The location

($x=-0.1, y=0.1, z=-0.4$) of the resulting J_{\min} ($SLI_{\max}=1.63$) can be observed in the left region, represented by the high values (red) in the color scale. The method seems to lateralize the seizure but anatomically the resulting location cannot represent a true epileptic source, as it is not localized in the brain volume. Moreover, the value obtained for the SLI_1 (< 2) indicates a poor fit. As shown in Chapter 3, this method fails in the case of multiple sources.

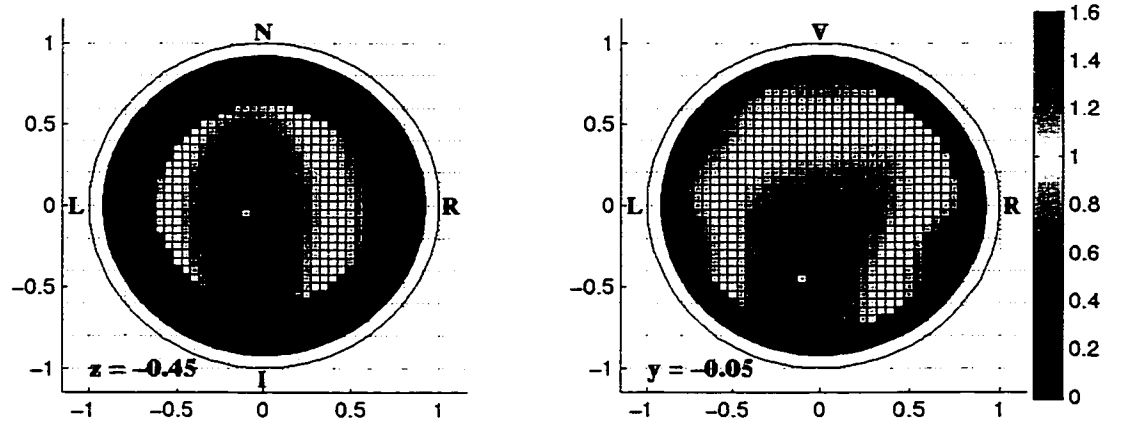


Figure 4.9. The Source Location Index distribution on the horizontal and vertical slice containing the minimum using the Single Dipole Fitting Method

4.4.2.2 Multiple Dipole Fitting

The second method applied is MUSIC, modified to use CSPs. The first three Common Spatial Patterns C_s , for which the variances accounted for in the ictal EEG are written in bold characters in Figure 4.5, are used to minimize the function in equation 2.42

The objective is to minimize the projection of the unit source $\hat{\mathbf{M}}$ of analytically determined orientation $\hat{\mathbf{a}}$, at each grid point, on the left null space of the CSPs \mathbf{C}_s , thought of as spanning the signal space. The SLI is calculated at each grid point as in equation 2.50 and its topography on both horizontal and vertical slices containing the maximum values of the SLI_2 is shown in Figure 4.10.

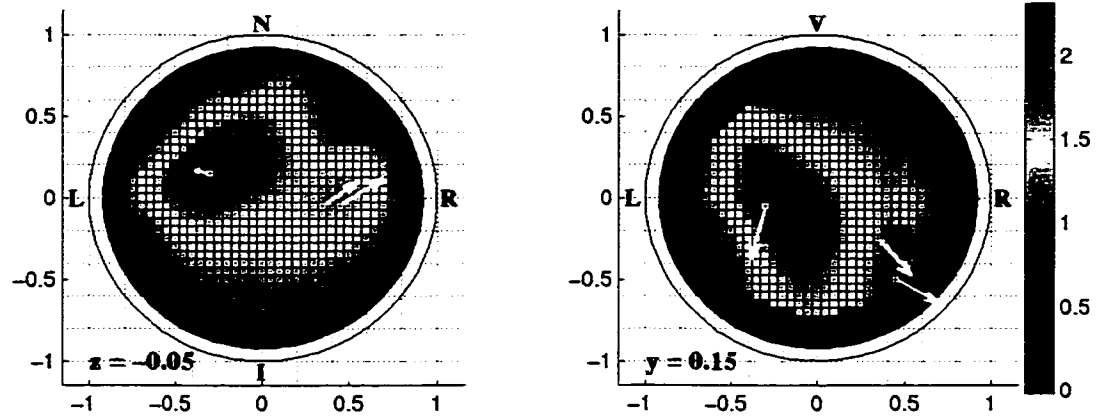


Figure 4.10. The Source Location Index distribution on the horizontal and vertical slice containing the minimum using the Multiple Dipole Fitting Method

The locations of the resulting peaks can be identified at $x=-0.3, y=0.15, z=-0.05$; $x=0.35, y=-0.05, z=-0.25$; $x=0.45, y=-0.05, z=-0.5$ and the corresponding SLI_2 are, in order, 2.29; 1.78; 1.65. The arrows at the three locations represent the orientations of the unit sources that best fit the data, analytically determined as in Chapter 2.

It can be observed that the highest SLI, which lateralizes the seizure focus on the left temporal lobe, is much greater than the two peaks located on the right side. The smaller values of the SLI for these last peaks would indicate either secondary sources or sources that are not dipoles or are not even located in the brain. Their location is improbable to represent an epileptic source, knowing the brain anatomy, even considering the localization error introduced by using a spherical model for seizure data. The later source is presumably a source of movement artifacts, resulting from the patient's movements during the seizure; it may be an artifact that lies within the same frequency range as the epileptic signal and for this reason could not be filtered out.

4.4.2.3 *LORETA*

The estimated LORETA solution \mathbf{i}_s is found from equation 2.64 where \mathbf{T} is the model dependent matrix, calculated for the upper half of the sphere, \mathbf{C}_s represents the three Common Spatial Pattern components selected as spanning the abnormal signal space, and Ψ_{as} is the corresponding eigenvalue matrix. The dimension of \mathbf{T} is $3G \times 24$, with the number of grid points $G=1346$, \mathbf{C}_s is 24×3 and Ψ_{as} is 3×3 . The source current density for each grid point (x, y, z) is the sum of three consecutive elements of \mathbf{i}_s , corresponding to x, y and z respectively.

$$i(x, y, z) = \text{sum}_3 [i_s(x, y, z)] \quad 4.3$$

Equation 4.3 is another form of equation 2.65. The source localization result obtained using LORETA on the real seizure EEG data is illustrated in Figure 4.11.

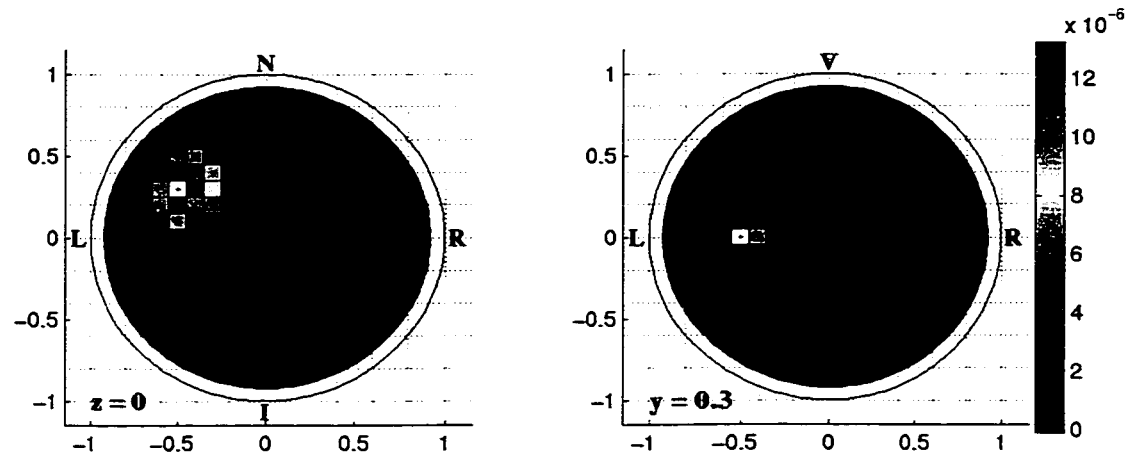


Figure 4.11. The horizontal and vertical slice topography of the LORETA solution

The estimated source location using LORETA is, for this patient, $x=-0.5$, $y=0.3$, $z=0$ which confirms the left anterior temporal origin of the seizure focus. Compared with the result obtained with MUSIC, LORETA locates the source 1-2 cm more towards the surface of the head.

4.4.3 Seizure Spread

The results show that there is a main seizure focus on the left side of the brain, with some right involvement. The question is whether the source on the right side is also responsible for the seizure onset, and if it is to what degree, or is it simply the spread of the epileptic activity from the left to the right side of the brain within the two seconds: the seizure spread may occur in fractions of seconds after the seizure onset (Tyner et al., 1983).

To get more insight into this problem, the Principal Component decomposition is applied to successive one second epochs of the ictal segment of the spatially and temporally filtered EEG in Figure 4.6, and then localizing the resulting spatial components with the MUSIC algorithm.

The next figure is the result of localizing all of the resulting principal components of four successive 1 sec ictal epochs, in the attempt to observe all of the sources responsible for the ictal activity, as time progresses. The title of each subplot represents the time limits of each EEG epoch in the ictal segment, in seconds.

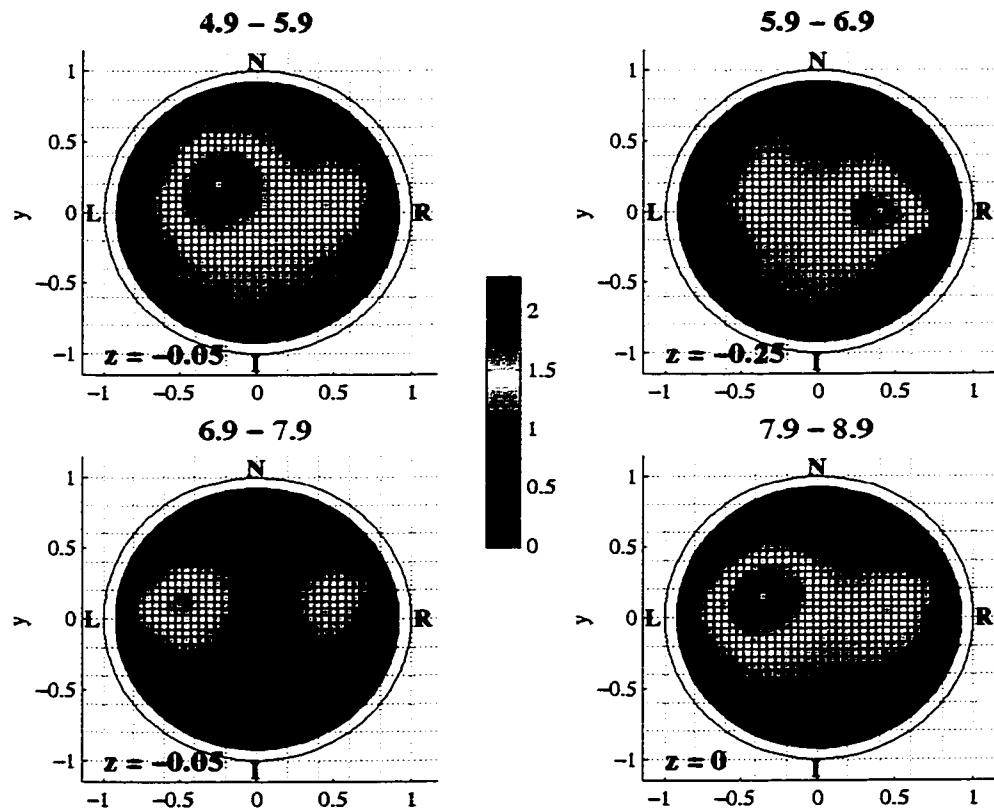


Figure 4.12. The SLI dynamics in the first four seconds of the seizure

The localizations resulted in acceptable peaks, greater than 2, only in the left-anterior side of the sphere. The second source is more active between 5.9-6.9 sec. The dynamics of the

source locations shows a transfer of the activity from the left side to the right side. One can observe that in the third second of the seizure, the main source is again located in the left, with reduced activity in the right side, this effect being accentuated as the time progresses. It can then be concluded that the second source, localized and shown in Figure 10 is an epileptic source whereas the third source is probably a source of artifact and is not localized in the sphere.

Overall, the results show a left antero-mid-temporal seizure, with some spread to the lower region of the right temporal lobe.

4.5 Validation of Results

The patient presented in this work had complex partial seizures for 17 years that could poorly be controlled with multiple medication. The MRI scans revealed a left temporal mesial lesion. The dissection of the medial temporal lobe revealed tough, fibrous tissue in the region of hippocampus and its anterior proximity, uncus.

The depth EEG recordings, performed during the operation, showed extensive electrical activity, spikes, occurring medially of the anterior temporal lobe: between 3 to 5 cm posterior to the anterior tip of the temporal lobe. The patient underwent left anterior temporal lobectomy in 1997, and is now seizure free. The results using both MUSIC and LORETA algorithms confirm the left temporal origin of the seizure onset.

5 DISCUSSION

The results in this work have shown that the nonorthogonal spatial components resulting from the Common Spatial Pattern decomposition of the data matrix are better for isolating the signal space of interest and produce more accurate source localizations than when the Principal Components are used.

The simulations show an example where, from a set of uncorrelated sources, a normal dipole source accounts for the maximum variance in the abnormal EEG and as a result the first PC in the EEG decomposition is misassigned to the abnormal source space of interest. If a single candidate source is projected onto the left null space of all the eigenvectors that correspond to eigenvalues different from zero, it is shown that all the sources, normal and abnormal, responsible for the EEG are correctly localized. However, no conclusion can be drawn, without prior knowledge about the origin of the sources, which is the case in practice, about which determined locations correspond to abnormal sources.

It was demonstrated that the first PC points along the direction of maximum variance in the EEG. Due to the constraint that the rest of the eigenvectors be orthogonal, their orientations depend on the orientation of the first. If the signal space is selected as in the MUSIC algorithm, as spanned by the first eigenvectors corresponding to the first eigenvalues significantly greater than zero, the abnormal signal space is not correctly isolated and the abnormal sources can not be localized. Instead, from the common spatial patterns, which form a non-orthogonal set of basis vectors determined from the covariance matrices of the abnormal and normal EEGs, the abnormal source space can be correctly selected. The selection of the basis vectors that span the source space of interest is made from common

basis vectors to both abnormal and normal EEGs resulting from CSP decomposition also on the basis of the variance accounted for in the EEG. The difference from the PC signal space selection used in MUSIC algorithm is that the signal vectors from the CSP decomposition of the EEG account for maximum difference in variance accounted for in the abnormal and normal EEGs. The basis vectors that account for minimum difference in variance in the abnormal and normal EEG span the background source space which is not of interest, and which is modeled as noise space.

One main challenge in successfully applying the CSP decomposition for signal subspace selection in the case of real data is finding the two EEG epochs, normal and abnormal, in other words localizing the moment in time when the abnormal sources become active. For the case of seizure data this is critical, as the aim is to localize the seizure focus. The method of temporal localization of the seizure onset used in this work is based on CSP decomposition of the EEG and the MUSIC algorithm. First the whole seizure data is filtered with a low pass filter such that only the frequencies below 20 Hz are retained. Second, the frequency-filtered data is visually inspected and the temporal region where a significant change in amplitude and perhaps in frequency or/and phase is determined. It is highly unlikely that the seizure onset can be determined precisely only by visual inspection. Therefore the seizure onset is successively assumed at different times in the determined region, the abnormal and normal EEGs selected as three-second epochs before respectively after the assumed seizure onset and CSP decomposition of the six second EEG performed. The modified MUSIC algorithm presented in this work is applied by projecting a candidate source on the left null space of the selected CSP signal vectors. The seizure onset is then assumed to be at the moment in time for which the error J_2 , calculated as in equation 2.47, is minimum. Third, in the attempt to reduce

the artifacts that may occur during the seizure the process is repeated for a band pass filter with different frequency limits, with more care for the low frequency limit as the seizure temporal patterns usually lie within a low frequency band. The last step concerns the fact that the seizure can start in one side of the brain and spread in fractions of seconds after the seizure onset to other areas of the brain. Choosing the length of the abnormal epoch becomes important for this reason. In order to determine the length of the abnormal epoch, the time segments around the seizure onset are symmetrically scanned starting with a maximum length of three-second normal and abnormal epochs, and each time the CSP decomposition and MUSIC is applied as before until the smallest J_2 is obtained. Once the seizure onset, the frequency band of the band pass filter and the length of the normal and abnormal epochs are found, the temporal and spatial filter is applied to a larger EEG segment that includes the two epochs in order to better visualize the evolution in time of the EEG produced by the abnormal signal sources of interest in both pre-ictal and ictal stage. As it results, the appeal of this method of seizure onset localization lies in the validity of the results, verified by clinical and imaging methods. As the focus of this research has been on methods of source localization, the temporal filtering method developed here came as a necessity for advancing the source localization methods for actual data, and it involves rather artisan work. The challenge lies in optimizing this method in order to reduce the tediousness of all of the steps involved.

The results in this work have also shown that the modified MUSIC and LORETA algorithms, applied to multiple time slices, are effective for multiple source localization whereas the Single Dipole Fitting fails. The Single Dipole Fitting involves scanning the brain volume with a candidate source and calculating at each grid point the projection of the data on

the left null space of this candidate source. This is equivalent to projecting the scaled eigenvectors resulting from the PC decomposition on the left null space of the candidate source. This method results in the localization of an equivalent dipole located towards the source of maximum variance. For the simulated EEG this can be explained by the fact that the first eigenvector accounts for 57% of the total variance in the EEG. The simulations show that projecting the whole set of eigenvectors on the left null space of the candidate source results in the same location as projecting only the signal eigenvectors, with a higher peak when only two eigenvectors are used. This result is not surprising as the first two eigenvectors account for more than 88% of variance accounted for in the abnormal EEG. This indicates that this method would result in a peak close to the location of an abnormal source if this source would account for considerably more variance compared to other sources that would generate the abnormal EEG, thought of as noise. The method applied to the real seizure data also shows the localization of an equivalent dipole and that the method fails as the predicted location is not in the brain volume. The SLI obtained using this method is smaller than 2 for real data and smaller than 3 for simulated data. The higher peak obtained in simulations is very probably obtained due to the lack of noise in the EEG and the use of the head model for both forward and inverse problems. For these reasons the GOF was set to 0.999 for simulations and consequently the $SLI > 3$. Using more dipole models in the projection matrix and scanning the head successively with only one dipole while the others are kept fixed would result in minima at the locations where the eigenvectors give a good approximation to the dipole models. This method of localizing multiple dipoles, not shown in this work, has two disadvantages: one disadvantage is the high computational cost; the other disadvantage is that it is based on the PC decomposition, which has been shown to be unreliable for the selection

of the signal space. This last disadvantage could be overcome by using the CSP decomposition, instead.

The MUSIC algorithm involves scanning the brain volume and projecting, at each grid point, a single candidate source on the left null space of the signal vectors derived from the covariance data matrix and directly calculating the orientation and the dipole moment that results in minimum error. The error is minimum at each location where one of the spatial components from the projection matrix approximates the linear combination of the columns of the transfer matrix, with coefficients given by the orientation vector.

The original MUSIC algorithm applied to EEG uses as signal vectors the first principal components of the data. As shown, these orthonormal spatial components can fail to correctly describe the source space of interest. In the simulated EEG an example of when the PC components fail to describe the abnormal source space is given and it is shown that neither the set of selected signal vectors nor the set of corresponding waveforms describes the whole set of abnormal sources. In this example it happens that the second principal component approximately describes the second source image and therefore this abnormal source is localized within an error of only 0.5 cm.

The modified MUSIC algorithm applied in this work is different from the MUSIC algorithm referred to in the previous paragraph in the sense that the candidate source is projected on the left null space of a set of nonorthogonal components resulting from the CSP decomposition of the data. This is effective since the background components can be chosen as being in the left null space of the signal vectors and are therefore modeled as noise

components. It results that the projection matrix is the key to the success in applying this method.

The main appeal of the MUSIC algorithm is that the projection matrix can be pre-calculated at each location and only the minimum eigenvalue and the corresponding eigenvector of a 3×3 matrix has to be determined. In this work it has been demonstrated that this eigenvector is the best orientation of the candidate source that minimizes its projection on the left null space of the data and the eigenvalue is the minimum error in this projection at the grid location. This suggests that the number of parameters that has to be found by trial and error is reduced to three (the location parameters) instead of six (three location parameters, two orientation parameters and one moment). The result is that the scanning for the source localization of multiple sources can be performed with practically no computational difficulties even for a finer grid than the one used in this work.

In the simulations presented in this work, the localization of the abnormal sources using the CSP signal vectors in the MUSIC projection matrix shows that the peak for the distributed source is not maximum. In other words, the error J_2 is not as close to zero as for the abnormal dipole source. As the dipole sheet is a set of closely spaced, synchronously active dipole sources, the best fit is found for an equivalent dipole placed in the vicinity of the distributed source.

On the other hand LORETA, which is not dependent on the source model or on the correlation between current sources, gives a blurred solution and localizes better the dipole sheet than the dipole source. Evidently, the low spatial resolution results in a lower peak. The dipole source is poorly localized with LORETA due to the low resolution of the method.

Several aspects related to source localization have been studied and not addressed in this work. One aspect concerns the location of the sources with respect to the grid points. In the simulated EEG, both dipole sources, the normal and the abnormal, are simulated such that they are located at grid points. Not described simulations showed that the localization of the noise free dipole sources not on the grid using MUSIC results in low peaks at grid locations in the vicinity of the simulated dipole source. It has been observed that the SLI topography of the radial dipole sources located off the grid show sharper peaks compared to the SLI topography for the tangential dipoles for which the peak is broader and flatter. The grid refinement of the volumes around the peaks revealed sharp peaks at the dipole source locations. However, in the presence of noise it was found that the grid refinement does not produce sharper peaks at the true source locations. If the PC is used in the projection matrix, the flat peak in this case is predominantly the result of the presence of noise components in the signal space.

Another aspect, which is not presented in this work, is the influence of the number of electrodes on source localization. Simulations have been done to get some insight into this problem. The main conclusion is that for dipole sources located on the grid, in the absence of noise, the SLI topography contains false peaks when the number of electrodes is smaller than the number of sources times the number of source parameters. For sources simulated in a sphere it was found that the minimum number of electrodes necessary for each source to be localized is six. The 24 electrode configuration is therefore acceptable both for the case of the three simulated sources, and for real data where the dimension of the signal space was estimated as being three. It was also found that if the electrode density differs on the surface, even for a number of electrodes of six times the number of sources, it is still possible to find

false peaks in the regions towards the small electrode density. This effect is accentuated in the case of dipole sources generated off the grid, when, in the absence of noise, refining the grid helps to enhance the SLI at the source locations. This is useful even if the number of electrodes is smaller than required.

The main conclusion is that the source localization of the EEG sources is feasible either by using the MUSIC algorithm or the LORETA method, subject to the correct selection of the signal subspace. It was found that the CSP decomposition better approximates the spatial and temporal patterns of the EEG model than the PC decomposition and is more effective in the selection of the signal space.

6 CONCLUSIONS

This work described, and applied methods of estimating the set of parameters that represent the sources of EEG. As an example, a forward model with two dipole sources (one considered as normal, relatively close to the surface, and one deep, abnormal) and a dipole sheet (also abnormal) in a three shell spherical model was simulated. Two approaches to decomposing the EEG and their effectiveness for source localization were presented.

The simulation results showed that the Principal Component decomposition of the EEG is ineffective for isolating the sources of interest (abnormal). It was shown that the Common Spatial Pattern decomposition gives a better approximation of the forward model and therefore this decomposition is more effective to use in source localization.

Three source localization algorithms, Single Dipole Fitting, Multiple Source Localization (MUSIC) and LORETA, were presented. The simulations performed using the three methods indicate that the Single Dipole Fitting is ineffective in the case of data produced by more than one source, as is generally the case in practice. On the other hand, MUSIC and LORETA methods correctly localize the sources of interest when used with the CSP decomposition of the EEG. However, it is shown that the Multiple Source Localization localizes better the single dipole sources, whereas LORETA gives better results for localizing distributed sources.

One example of seizure data was chosen in this work to illustrate the practical application of the EEG spatio-temporal decomposition and the localization of the epileptic focus. The data was temporally and spatially filtered using methods based on the CSP decomposition in order to determine the seizure onset and to isolate the spatio-temporal patterns of interest from the noise and background activity present in the EEG recording. MUSIC and LORETA

using the CSP decomposition correctly lateralized the seizure focus whereas the Single Dipole Fitting failed. The dynamics of the seizure were also presented, and correlated to the clinical findings.

The results show that it is possible to determine the electrogenesis of the neural activity of interest, without any prior knowledge about the number of sources in the signal space, by using the Common Spatial Pattern Decomposition of the EEG with the Multiple Source Localization - MUSIC, or LORETA method. In order to obtain accuracy, however, a more realistic head model calculated for each patient, based on MRI and CT data, should be used.

BIBLIOGRAPHY

- Alibadi, M. H., Brebbia C. A., Advanced Formulations in Boundary Element Methods, Computational Mechanics Publications, Southampton, UK, 1993.
- Arnold, D. L., Clinical Application of Magnetic Resonance Spectroscopy in Neurological Disorders, The Physics of MRI, 1992, AAPM Summer School Proceedings, Editors Bronskill, Michael, Sprawls, Perry-Editors, American Association of Physics Monograph No. 21, Published by The American Institute of Physics, Inc., NY, pp. 571-578, 1993.
- Ary, J. P., Klein, S. A. and Fender, D. H. Location of sources of evoked scalp potentials: corrections for skull and scalp thickness. IEEE Trans. Biomed. Eng, BME-28: 6: 447-452, 1981.
- Brebbia, C. A., Walker, S., Boundary Element Techniques in Engineering, Newnes-Butterworths, London, 1980.
- Brogan, W., Modern control theory. Prentice Hall, Englewood Cliffs, 1991.
- Cascino, G. D., Magnetic Resonance Imaging in Frontal Lobe Epilepsy, *Epilepsy and the Functional Anatomy of the Frontal Lobe*, edited by H. H. Jasper, S. Riggio, and P. S. Goldman-Rakic, Raven Press, New York, Advances in Neurology, 66: 199-211, 1995.
- Dezortova, M., Hajek, M., Fendrych, P., Rolencova, E., ¹H MR Spectroscopy as a routine tool for the lateralization of the epileptogenic focus. Proceedings of the sixth scientific Meeting and Exhibition of the International Society for MR in Medicine, Sydney, Australia, April 18-24,1998.

- Fletcher, D., Amir, A., Jewett, L., Fein, G., Improved Method for Computation of Potentials in a Realistic Head Shape Model, *IEEE Trans. Biomed. Eng.*, 42, 1094-1103, 1995.
- Fukunaga, K., Introduction to statistical pattern recognition. Academic Press, New York, 1972.
- Gevins, A., High-Resolution Electroencephalographic Studies of Cognition, *Epilepsy and the Functional Anatomy of the Frontal Lobe*, edited by H.H. Jasper, S. Riggio, and P. S. Goldman-Rakic, Raven Press, Ltd., New York, *Advances in Neurology*, 1995; vol. 66: 181-198.
- Gevins, A., The future of Electroencephalography in Assessing Neurocognitive Functioning, *Electroeneph. clin. Neurophysiol.*, 106: 165-172, 1998.
- Gorodnitsky, I. F., George, J. S. and Rao, B. D. Neuromagnetic source imaging with FOCUS: a recursive weighted minimum norm algorithm. *Electroeneph. clin. Neurophysiol.*, 95: 231-251, 1995.
- Halmos, P. R., Finite-dimensional vector spaces, Springer-Verlag, New York, Heidelberg, Berlin, 1974.
- Hammer B. E., Christensen N. L., Raylman R. R., MR-PET: Sub-millimeter MR and PET image in the same scanner, *Proceedings of The Sixth Scientific Meeting and Exhibition of The International Society for MR in Medicine*, Sydney, Australia, April 18-24, 256, 1998.

- Haueisen, J., Ramon, C., Czapski, P. and Eiselt, M. On the influence of volume currents and extended sources on neuromagnetic fields: a simulation study. *Annals of Biomedical Engineering*, 23: 728-739, 1995.
- Hendelman, W. J., *Student's Atlas of Neuroanatomy*, W. B. Saunders Company, Philadelphia, USA, 1994.
- Ives, J. R., Warach, S., Schmitt, F., Edelman, R.R., Schomer, D. L. Monitoring the patient's EEG during echo planar MRI. *Electroenceph. clin. Neurophysiol.*, 87:417-420, 1993.
- Jager, L., Hoffmann, A., Joppich, M., Reiser, M., Simultaneous EEG recording with MR data-acquisition, *Proceedings of The Sixth Scientific Meeting and Exhibition of The International Society for MR in Medicine*, Sydney, Australia, April 18-24, 1998; 286
- Koles, Z. J. The quantitative extraction and topographic mapping of abnormal components in the clinical EEG. *Electroenceph. clin. Neurophysiol.*, 79: 440-447, 1991.
- Koles, Z. J. Trends in EEG source localization. *Electroenceph. clin. Neurophysiol.*, 000: 1-11, 1997.
- Koles, Z. J., Lind, J. C. and Soong, A. C. K. Spatio-temporal decomposition of the EEG: a general approach to the isolation and localization of sources. *Electroenceph. clin. Neurophysiol.*, 95: 219-230, 1995.
- Koles, Z. J., Soong, A. C. K., EEG source localization: implementing the spatio-temporal decomposition approach. *Electroenceph. clin. Neurophysiol.*, 000: 1-10, 1998.

- Krakow, K., Allen, P. J., Polizzi, G., Lemieux, L., Fish, D.R., The amplitude and distribution of EEG pulse artifact in the MR scanner: its effect on the detection of EEG events. Proceedings of The Sixth Scientific Meeting and Exhibition of The International Society for MR in Medicine, Sydney, Australia, April 18-24, 1998.
- Kuzniecky, R. I., Jackson, G. D., Magnetic Resonance in Epilepsy. Raven Press, New York, USA, 1995
- Lazeyras, F., Seeck, M., Michel, C. M., EEG recording during MR examination for presurgical evaluation of epilepsy. Proceedings of The Sixth Scientific Meeting and Exhibition of The International Society for MR in Medicine, Sydney, Australia, April 18-24, 1998; 744.
- Lin, J. C., Gates, J. R., Ritter, F. J., Dunn, M. B., Neves, C. M., Nelson, C. A., Truwit C. L., Lateralization of epileptic focus in temporal lobe epilepsy patients using Proton MR Spectroscopy, Proceedings of The Sixth Scientific Meeting and Exhibition of The International Society for MR in Medicine, Sydney, Australia, April 18-24, 1998; 1512, 1998.
- Mosher, J. C., Leahy, R. M. Recursive MUSIC: a framework for EEG and MEG source localization, IEEE Trans. Biomed. Eng., BME- 45: 1342-1354, 1998.
- Mosher, J. C., Lewis, P. S. and Leahy, R. M. Multiple dipole modeling and localization from spatio-temporal MEG data. IEEE Trans. Biomed. Eng., BME-39: 541-557, 1992,.
- Myers, D. G., Psychology, Worth Publishers, New York, USA, 1995
- Nunez P. L., Katznelson R. D., Electric fields of the brain, University Press, Oxford, 1981.

- Pasqual-Marqui, R. D., Michel, C. M. and Lehmann, D. Low resolution electromagnetic tomography: a new method for localizing electrical activity in the brain. *International Journal of Psychology*, 18: 49-65, 1994.
- Penrose, R., A generalized inverse for matrices, *Proceedings of the Cambridge Philosophical Society*, vol. 51, part 3: 406-413, 1955.
- Rao, C. R., Mitra, S. K., Theory and application of constrained inverse of matrices. *SIAM J. Appl. Math.*, 24: 473-488, 1973.
- Roth, B. J., Balish, M, Gobrach, A. and Sato, S., How well does a three-sphere model predict positions of dipoles in a realistically shaped head? *Electroenceph. clin. Neurophysiol.*, 87:175-184, 1993.
- Shen, J., Shungu, C., Dikoma, Rothman L. D., Chemical Shift Imaging of GABA in the Human Brain, *Proceedings of The Sixth Scientific Meeting and Exhibition of The International Society for MR in Medicine*, Sydney, Australia, April 18-24, 627, 1998.
- Sherg, M. and von Cramon, D. Evoked dipole source potentials of the human auditory cortex. *Electroenceph. clin. Neurophysiol.*, 65: 344-360, 1986.
- Soong, A. C. K. and Koles, Z. J., Principal-component localization of the sources of the background EEG. *IEEE Trans. Biomed. Eng.*, BME-42: 59-67, 1995.
- Srebro, R., Iterative refinement of the minimum norm solution of the bioelectric inverse problem. *IEEE Trans. Biomed. Eng.*, BME-43: 457-552, 1996.
- Strang, G., *Linear algebra and its applications*. Academic Press, Orlando, 1980.

- Symms, M. R., Allen, P. J., Woermann, F. G., Polizzi, G., Krakov, K., Barker, G. J., Fish, D. R., Duncan, J. S., Reproducible localization of interictal epileptiform discharges using EEG-correlated fMRI, Proceedings of The Sixth Scientific Meeting and Exhibition of The International Society for MR in Medicine, Sydney, Australia, April 18-24, 1998.
- Tyner, F.S., Knott, J.R., Mayer, W.B. Jr., Fundamentals of EEG technology. New York, Raven Press, 1983.
- van Drongelen, W., Yuchtman, M., Van Veen, B.D. and van Huffelen, A.C. A spatial filtering technique to detect and localize multiple sources in the brain. Brain Topogr., 9:39-49, 1996.
- Webster, J. G., Medical Instrumentation, Houghton Mifflin Company, Boston, USA, 1992.
- Wong, P. K. H., Digital EEG in clinical practice. Lippicott-Raven, Philadelphia. New-York, 1996.
- Yan, Y., Nunez, P. L. and Hart, R. T. Finite-element model of human head: scalp potentials due to dipole sources. Med. Biol. Eng. Comput., 29:475-481, 1991.
- Yvert, B., Bertrand, O., Echallier, J. F., Pernier, J., Improved forward EEG calculations using local mesh refinement of realistic head geometries, Electroencephalography and clinical Neurophysiology, 1995, 95, 381-392.